

# ABSTRACT

Title of thesis: SOLVENT BEHAVIOR IN HYDROPHOBIC SILICA NANOTUBES  
AND NANOTUBE MEMBRANES

Karthik Jayaraman Master of Science, 2005

Thesis directed by : Professor Douglas S. English

Professor Sang Bok Lee

The development of template-synthesized silica nanotubes has created a unique opportunity for studying confined fluids by providing nanometer-scale containers in which, the inner diameter (i.d.) and surface chemistry can be systematically and independently varied. An interesting question to be answered is: Do solvents wet nanometer-scale tubes in the same way that they wet ordinary capillaries? To answer this question, we have conducted studies to explore the wettability of the hydrophobic interiors of individual nanotubes. In these studies, single nanotubes with i.d.'s of either 30 or 170 nm were investigated over a range of water/methanol mixtures. These studies provide a direct route for comparing wetting phenomena in nanotubes with conventional macroscopic theories of capillarity. Our observations reveal four important aspects of wetting in the sub-200 nm regime; (i) observation of a sharp transition between wetting and non-wetting conditions with increasing methanol concentration, (ii) invariance of this transition between nanotubes of 30 and 170 nm pore diameter (iii) failure of the Young-Laplace equation to accurately predict the methanol mole fraction for the transition and (iv) the reversibility of the observed wetting. The single nanotube measurements were complemented with membrane transport experiments that corroborate our conclusions. The first two aspects conform to conventional capillarity (Young-Laplace), but the latter two do not. The variation between the predicted and the experimental values may be associated with either our reliance on macroscopic values of contact angles and surface tensions in the Young-Laplace equation, or to liquid phase instability within the hydrophobic pore.

SOLVENT BEHAVIOR IN HYDROPHOBIC SILICA  
NANOTUBES AND NANOTUBE MEMBRANES

by

Karthik Jayaraman

Thesis submitted to the Faculty of the Graduate School of the  
University of Maryland, College Park in partial fulfillment  
of the requirements for the degree of  
Master of Science  
2005

Advisory Committee:

Professor Douglas. S English , Chair

Professor Sang Bok lee

Professor Neil V. Blough

©Copyright by

Karthik Jayaraman

2005

# ACKNOWLEDGEMENT

*Self-confidence is the first requisite to great undertakings.- Samuel Johnson*

I extend my sincere thanks to Prof. Douglas S. English and Prof. Sang Bok Lee for being my research advisors for the last two years and for challenging my thinking, writing and research skills. I also record my sincere thanks with warmth to them for providing me valuable guidance, resources and encouragement throughout this work. I must admire Prof. English for pulling me up occasionally for my laxity and profusely thank him for such lashes which enabled me to be on guard with regard to my ultimate accomplishment. I would like to thank Prof. Neil V. Blough for his willingness to share his research expertise by being a part of my thesis examining committee. My genuine gratitude goes to Dr. Kenji Okamoto and Dr. Sang Jun Son for their assistance in helping me to comprehend the concepts and techniques to carry out the research. I would like to thank Xiang Wang, Charles Lockett and all other lab members (English and Lee group) for their valuable support in the lab and for providing a friendly atmosphere. My profound acknowledgment goes to the University of Maryland, College Park in specific the Department of Chemistry and Biochemistry, which has been a great place of effective learning for me. I would like to express my appreciation for the constant support, understanding and love that I received from my parents, brother and friends during the past years. Finally, but not perfunctorily, I thank the Almighty for giving me such a great opportunity.

# TABLE OF CONTENTS

List of Tables	vi
List of Figures	vii
Chapter I: Introduction	1
1.1 Background	1
1.2 Focus	2
1.3 Outline	2
Chapter 2: Literature Review	4
2.1 History of Nanotechnology	4
2.2 Nanomaterials	6
2.2.1 Nanotubular structures	7
2.2.2 Nanotubes: synthetic techniques	7
2.3 Silica Nanotubes using template synthesis	9
2.3.1 Silica	9
2.3.2 Template Synthesis	9
2.3.3 Sol-gel process	10
2.3.4 Template Surface Sol-Gel (SSG) synthesis	11
2.3.5 Applications of template synthesized nanotubes	15
2.4 Nanotube Characterization	15
2.5 Laser Scanning Confocal Fluorescence Microscopy	17
2.5.1 Confocal Microscopy	17
2.5.2 Fluorescence Microscopy	18
2.6 Fluorescence Recovery After Photo Bleaching	18
2.7 Solvatochromism	21
2.8 Wetting and Capillarity	23
2.8.1 Contact angle and surface tension	23
2.8.2 Laplace equation and capillarity	24
2.8.3 Nanoscale Capillarity	26
2.9 Hydrophobic Effects or Interactions	26

2.9.1 Length scale hydrophobic effects	27
2.9.2 Theoretical predictions on hydrophobic effect/Solvent confinement in hydrophobic environments	29
Chapter 3: Experimental details	31
3.1 Synthesis of Silica Nanotubes	31
3.2 Single Nanotube measurements	34
3.2.1. Fluorophore adsorption	34
3.2.2 Sample Preparation for FRAP experiments	34
3.2.3 FRAP Experiments	36
3.2.3.1 Fast recovery FRAP measurements	37
3.3 Spectroscopic imaging (Solvatochromic Experiments)	40
3.4 Image analysis	41
3.5 Transport experiments	41
3.6 Materials used	42
Chapter 4: Results and Discussions	44
4.1 Results	44
4.1.1 FRAP Studies	45
4.1.2 Spectroscopic Imaging	47
4.1.3 Observing Capillary Wetting	51
4.1.3.1 Nanotube Defects and Anomalous Wetting	52
4.1.4 Membrane Transport Experiments	54
4.1.5 AC Impedance Measurements	55
4.2 Discussion	58
Chapter 5 : Conclusions and Future Work	62
5.1 Conclusions	62
5.2 Future work	63

Appendix	64
A. Procedure to conduct FRAP Experiments	64
B. Procedure to perform spectroscopic imaging.	65
C . IGOR routines for loading and manipulating microscope images	66
C1.IGOR routine for loading and manipulating microscope images.	67
C2. IGOR routine for loading and manipulating spectrums obtained from CCD camera for solvatochromic experiments.	74
C3. IGOR routine for obtaining FRAP recovery curve and diffusion coefficients.	82
References	92

# LIST OF TABLES

<b>Table 1.</b>	Synthesis routes of various inorganic nanotubes.	<b>8</b>
<b>Table 2.</b>	Fluorescence Recovery After Photobleaching Considerations.	<b>20</b>
<b>Table 3.</b>	Steps involved in sol-gel template synthesis of silica nanotube membranes	<b>33</b>
<b>Table 4.</b>	Molar extinction coefficients and maximum absorption wavelength values. ( $\lambda_{\max, \text{abs}}$ ) for DiIC <sub>18</sub> at various mole fractions of methanol in water	<b>42</b>
<b>Table 5.</b>	Contact angles of methanol/water mixtures on an OTS surface and the predicted capillary pressure for 30 and 170 nm nanotubes	<b>60</b>



# LIST OF FIGURES

Figure 1.	Schematic illustration of the research outline.	3
Figure 2.	Illustration of different Nanotechnology applications.	6
Figure 3.	Surface Sol-Gel synthesis of Silica Nanotubes.	12
Figure 4.	Electron micrographs : A) SEM image of CVD template synthesized nanotubes. B) TEM image of a SiO <sub>2</sub> nanotube. C) SEM image of gold nanoparticles nanotubes. D) TEM image of a PEDOT nanotube.	16
Figure 5.	Recovery After Photobleaching .	19
Figure 6.	Fluorescence emission spectra of Nile red in various solvents. For the spectrum in water a small proportion(2%) of methanol was added to aid dissolution	22
Figure 7.	Contact angles and extent of wettability.	24
Figure 8.	Laplace equation and capillarity phenomena (capillary rise in water and depression in mercury).	25
Figure 9.	(A)Schematic view of local water structure near a small hydrophobic sphere. Dashed lines indicate hydrogen bonds. (B)Schematic view of water structure near large parallel hydrophobic plates. Shaded area indicates regions where water density is essentially that of the bulk liquid; vacant regions indicate where water density is essentially that of the bulk vapor.	28
Figure 10.	Alumina templates with pore diameter of 60nm (A) Top view (B) Cross-sectional view).	32
Figure 11.	Schematic of sol-gel template synthesis of silica nanotubes	32

Figure 12.	Introduction of dye to the OTS-modified hydrophobic nanotube interiors. (A) OTS-modified silica nanotubes were stained with either DiIC18 or Nile red by physisorption to the hydrophobic interior surface. The surfactant-like fluorescent dye, DiIC18, was used in FRAP experiments, and the solvatochromic dye, Nile red, was used as a reporter of local dielectric properties inside individual nanotubes. Both dyes partition well to the hydrophobic interface and only trace amounts were used to ensure that the nanotube's internal surface properties were not significantly altered by the adsorbed dyes. (B) Step-by-step scheme showing the procedure for the introduction of DiIC18 to the nanotube interior. Nile red was introduced in an analogous manner.	<b>35</b>
Figure 13.	Illustration of FRAP in hydrophobic silica nanotubes.	<b>37</b>
Figure 14.	Schematic of modulating the laser beam using Acoustic Optical Modulator.	<b>39</b>
Figure 15.	Schematic of scanning confocal fluorescence microscope.	<b>40</b>
Figure 16.	(A) Schematic of membrane assembly and U-tube set up (B) Picture of actual U-tube experiment/	<b>43</b>
Figure 17.	Microscope images of differentially-modified silica nanotubes. (A) A TEM image of nanotubes with 30 nm i.d. and internally modified with OTS (B) Laser scanning confocal fluorescence image of a single 30 nm i.d. nanotube. The interior surface contains a trace amount of the fluorescent dye, DiIC <sub>18</sub> . Prior to imaging, the nanotube was immobilized on a glass coverslip under water.	<b>45</b>
Figure 18.	Examples of FRAP experiments conducted with 30 nm i.d. nanotubes under non-wetting conditions in water and strongly-wetting conditions in methanol. (A) Confocal fluorescence image of a DiIC <sub>18</sub> -bearing hydrophobic nanotube immersed in water just prior to conducting the FRAP experiment. The green arrows indicate four spots which were arbitrarily chosen for photobleaching. (B) A confocal image obtained 26 minutes after photobleaching was conducted showing that under pure water no FRAP is observed. The lack of diffusion-induced recovery suggests that the nanotube interior remains dry when	<b>49</b>

immersed in water as expected for a hydrophobic capillary. (C,D) Confocal images of a hydrophobic nanotube before and after conducting a FRAP experiment in methanol. Here, bleaching was conducted at a single spot shown by the green arrow. In contrast to the experiment conducted in water, a decrease in emission was observed over the entire nanotube interior. The wide-spread bleaching occurs because of rapid diffusion by DiIC<sub>18</sub> in the nanotube interior. As molecules are bleached, they rapidly diffuse away diluting the concentration of fluorophores over the entire nanotube. Facile diffusion in the nanotube indicates that hydrophobic nanotube interior has been filled by methanol. (E) Fluorescence recovery curve demonstrating the rapid recovery observed in pure methanol. This data was used to calculate the diffusion coefficient for DiIC<sub>18</sub> in the methanol-filled nanotube by using equations 1,2&4 . The calculated value is  $8.7 \times 10^{-7} \text{ cm}^2/\text{s}$ .

- Figure 19. Nile red fluorescence spectra acquired in different solvents and from a single silica nanotube. (A) Nile red emission in heptane, ethyl acetate, methanol and water. In water, a small proportion (2%) of methanol was added to aid dissolution. (B) Emission spectra from Nile red inside an OTS modified nanotube. The nanotube was initially immersed under water (—) and then under methanol (---). The spectrum acquired from the dry nanotube prior to the addition of water (data not shown) overlays well with the spectrum in water,  $\lambda_{\text{max}}$ . **50**
- Figure 20. Solvent-dependent wettability of 30 and 170 nm nanotubes. (A) Wettability of the hydrophobic nanotube interior over a range of methanol mole fractions for both 30 and 170 nm nanotube internal diameters. The transition from nonwetting to wetting conditions occurs between 0.31 and 0.57 methanol mole fraction for both nanotube sizes. (B) Wettability of both nanotube sizes after equilibration for 24 h. **52**
- Figure 21. FRAP experiment conducted in a nanotube (i.d. = 170 nm) immersed in a water/methanol mixture,  $X_{\text{MeOH}} = 0.31$ . (A) A sequence of fluorescent images taken during the FRAP experiment. (B) TEM showing a fragmented nanotube end. (C) Fluorescence intensity profiles taken along the nanotube before bleaching (red), after bleaching (blue) and after recovery (black). (D) FRAP recovery curves constructed from sequential images for point 1 (solid line) and point 2 (dotted line). **54**

Figure 22. Results from measurements made with an OTS-modified nanotube membrane (i.d. = 170 nm). (A) Comparison of results from solute transport studies(dotted line) with those from wettability studies(solid line) of individual nanotubes. (B) Semilogarithmic plot of the membrane resistance,  $R_M$ , over a range of  $X_{\text{MeOH}}$ .  $R_M$  values were determined from AC impedance measurements and were conducted in electrolytic solutions of 0.01 M KCl. The value of  $R_M$  is diminished by ion flow when the membrane pores are wetted and is dramatically increased when the hydrophobic membrane pores are dry. The sharp decrease in the value of  $R_M$  above  $X_{\text{MeOH}} = 0.31$  indicates that the membrane channels have filled. During the course of the experiment, methanol concentration was first increased and then decreased. Dewetting was observed as the mole fraction was decreased. 57

# Chapter 1: Introduction

## 1.1 Background

“Nano-” and “Bio-” are the favored prefixes in the scientific community in this day and age. However, the origin of bio-nanotechnology research can be dated back several decades. The current work is focused on tubes synthesized at a nanoscale and targeted for bio-medical applications including bio-molecular storage and delivery, targeted drug delivery and miniature reaction vessels. The work involves fluorescence microscopic techniques that can record information at the nano level and explain phenomena such as wetting and diffusion leveling this regime. Silica nanotubes are the promising competitive counterparts of carbon nanotubes and are easy to make and can be derived through well-known chemistry. Silica nanotubes can be readily suspended in an aqueous solution and can be easily modified for specialized applications thereby surpassing carbon nanotubes in several aspects. We have adopted the template synthesis technique pioneered by Martin and co-workers in the mid 1980's to synthesize silica nanotube membranes and nanotubes. A number of thorough investigations have to be performed before the synthesized silica nanotubes can be employed for the envisioned potential applications. One such study which is critical and challenging is; “Can we really get a solvent in and out of these nanotubes without any barrier”? To answer this question we have conducted wetting and diffusion studies in single nanotube and nanotube membranes using a range of water/methanol mixtures. Template synthesized silica nanotubes with hydrophobic interior are dressed with dye molecules to study the wetting and diffusion phenomena (i.e. to investigate whether a particular solvent can enter a

nanotube) using Fluorescence Recovery After Photobleaching (FRAP) experiments. Spectroscopic imaging with Nile Red, a solvatochromic probe, was done to acquire information on local dielectric properties inside single nanotube. Transport experiments with silica nanotube membranes were performed to understand the throughput and selectivity of these nanotube membranes.

## 1.1 Focus

The foci of this work are:

1. To synthesize well-defined rigid silica nano tubes of different sizes and surface chemistries using sol-gel template synthesis.
2. To employ silica nanotubes as tool to understand the behavior of nano-confined liquids, using scanning confocal fluorescence microscopy.
3. To investigate whether nanoscale wetting and capillarity concur with macroscopic wetting and capillarity.

## 1.3 Outline

In this work hydrophobic nanotubes membranes and single nanotubes were synthesized by sol-gel template synthesis. Fluorescence recovery after photobleaching experiments and spectroscopic imaging were performed on single nanotubes using scanning confocal fluorescence microscopy. FRAP measurements revealed information about the wettability of the hydrophobic silica nanotubes and the diffusion phenomena inside the hydrophobic interior. Solvatochromic experiments aided in understanding the dielectric

properties of the nanotube interior. Transport experiments and AC impedance measurements were performed using diffusion cell set-up on nanotube membranes. Finally single nanotube measurements were compared with ensemble measurements. These measurements were compared with theoretical predictions and simulations to understand the solvent behavior in confined hydrophobic environments. Figure 1 illustrates the schematic outline of the research work.

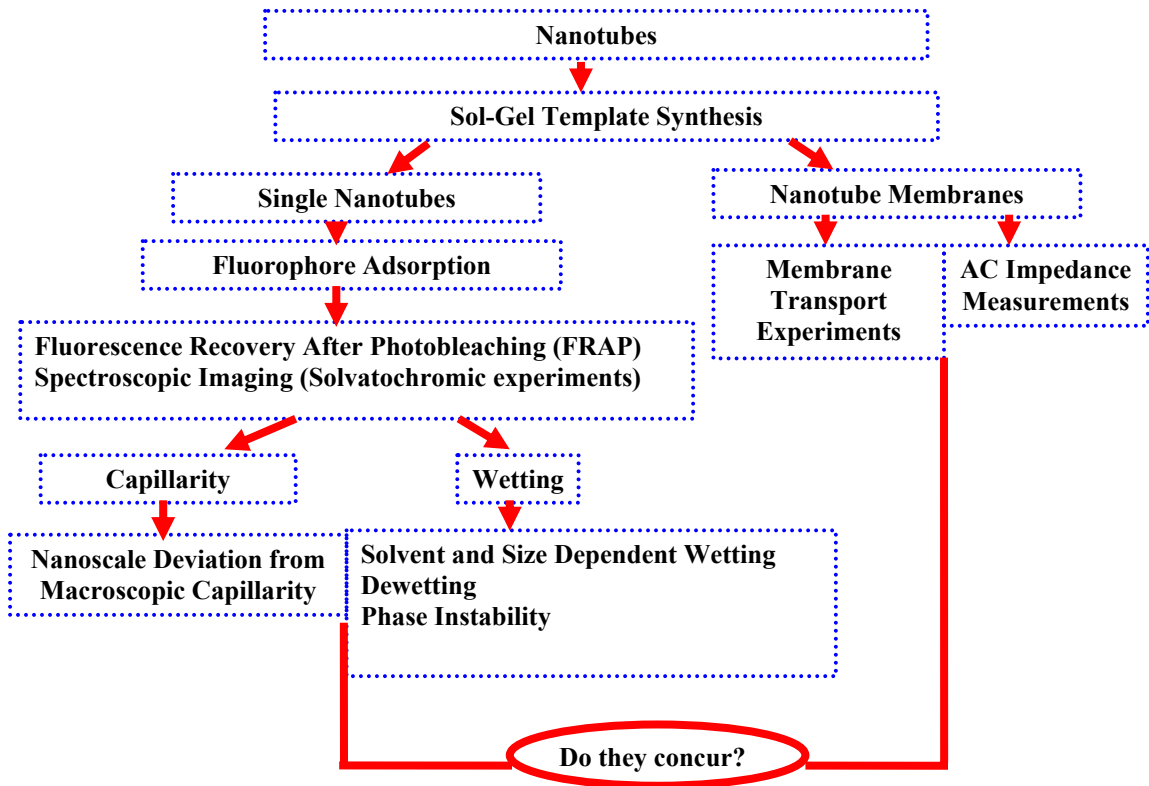


Figure 1. Schematic illustration of the research outline.

# Chapter 2: Literature Review

## 2.1 History of Nanotechnology

Over several decades and till today, ideas in chemistry, physics and biology have been shared and new advances are made in several areas including electronics, medicine, and materials science. The origin of nanotechnology dates back to the middle of 19<sup>th</sup> century with some milestones in the birth and evolution of nanotechnology<sup>1</sup> provided below:

- In 1857, Michael Faraday discovered colloid gold.
- In 1905, Albert Einstein provided a thoroughly quantitative theory for the state of a colloid dispersion.
- In 1932, Langmuir established the existence of monolayers (layers of atoms or molecules one atom thick)
- In 1958, Richard P. Feynman discussed the possibility of controlling materials at the level of atoms and molecules – this was the first vision of the possibilities of science and technology at the nanoscale.
- In 1974, the term ‘nanotechnology’ was coined by Norio Taniguchi of the University of Tokyo. The prefix ‘nano-’ being derived from the Greek word ‘*nanos*’, which means dwarf.
- In 1981, Gerd Binnig and Heinrich Rohrer invented the Scanning Tunneling Microscope (STM) at IBM.



- In 1985, Richard Smalley, Robert Curl and Harold Kroto discovered Buckminsterfullerene ( $C_{60}$ ) while investigating the outer atmosphere of stars, for which they were awarded the Nobel Prize in 1996.
- In the mid-1980's template synthesis technique which uses membranes with nano-sized pores as the foundation for growing nanostructures (silica, gold) was pioneered by Charles Martin.
- In 1991, Sumino Iijima discovered a process to make 'graphitic carbon needles ranging from 4nm to 30nm in diameter and 1 micron in length'. Carbon nanotubes were discovered
- In 1993, first high-quality quantum dots prepared.
- In 1997, Lucent Technologies fabricated the 'nanotransistor' – a complete metal oxide semiconductor transistor.
- In 2000, the first DNA motor was created by Lucent Technologies with Oxford University.
- In 2001, Nanohorns, irregularly shaped nanotubes, were developed as fuel cell for hydrogen-based fuel such as methanol.
- In 2002, clothing embedded with nanoparticles that produce a stain-repellent coating has been developed.
- In 2003, prototype nano solar cells were made by Nanosolar Inc. in California using conducting polymers and nano particles.
- In 2004, Nanospectra Bioscience has used gold-coated nanoshells to destroy cancer tumors in mice.

## 2.2 Nanomaterials

Nanomaterials are materials integrated with a nanoscale component such as nanoparticles, nanotubes, nanowires and nanorods that exert a great influence on properties or function.<sup>2</sup> Nanomaterials possess unique physical and chemical properties and can be used for a wide variety of applications including optical, electrical, mechanical and catalytic activity, biomedical, flat panel displays, medical implants and aerospace applications to name only a few.

Nanomaterials encompass nanoparticles and nanocrystal composites, nanoscale coatings and films, nanotube and nanowire composites. Enormous interest lies in using spherical nanoparticles for applications including biosensors, drug delivery and electronics.

Figure 2 depicts the various domains of nanotechnology.

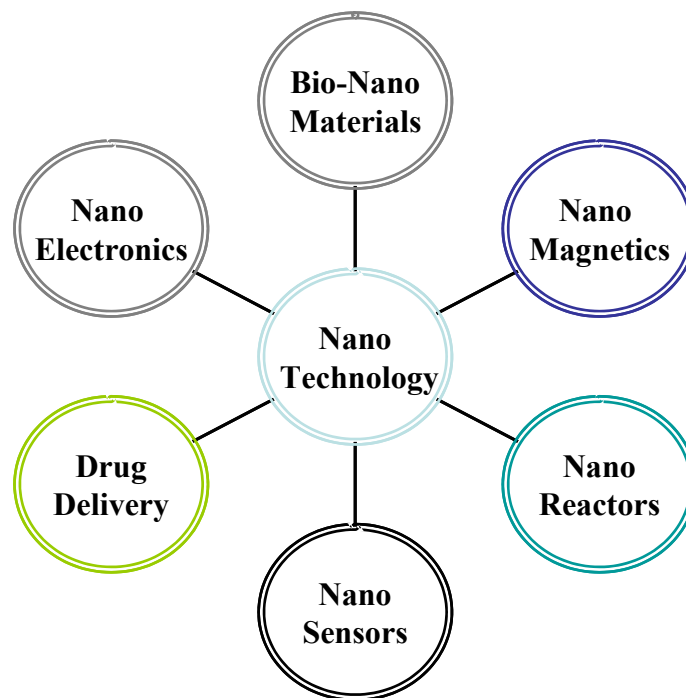


Figure 2. Illustration of different Nanotechnology applications.

Bio-Nano materials are materials integrated with a nanoscale component such as nanotubes and nanowires and that has application in the medical field and biological organisms. Nanoelectronics and nanomagnetics are nanotechnologies related to the miniaturizations of electronic and magnetic devices respectively leading to high performance electronic devices and development of powerful and higher capacity computer-driven devices. Drug delivery systems are nanostructures that can deliver drugs within the body to specific targets in nanovolumes efficiently. Nanosensing deals with using fluorescent nanoparticles and quantum dots to detect and identify biological molecules.<sup>1</sup> Nanoreactors involve using nanotubes as miniature reaction vessels to mimic biological reactions.

### *2.2.1 Nanotubular structures*

Tubular structures are well suited for many applications including chemical nano containers, miniature reaction vessels and bio-molecular storage, as they are hollow and the inner and outer surfaces can be differentially modified using various surface chemistries.<sup>3-6</sup> Single walled nanotubes have high aspect ratio and are extremely tough and strong. Nanotubular structures provide a simple system for molecular modelers or theoreticians to address interesting phenomena such as wetting, capillarity and condensation at the nanoscale.

### *2.2.2 Nanotubes: synthetic techniques*

Nanotubes, both from carbon and inorganic materials can be made through various techniques and they demonstrate a wide range of interesting properties. Carbon nanotubes

can be synthesized by high pressure CO conversion (HIPCO), pulsed laser vaporization (PLV), chemical vapor deposition (CVD) and Carbon Arc synthesis (CA). Inorganic nanotubes have emerged to become a group of novel materials. Inorganic nanotubes synthesis started with the layered metal chalcogenides, but eventually now other inorganic materials can also be prepared in the form of nanotubes, as demonstrated by the metal oxides. Various synthesis routes for nanotubes from metal chalcogenides is listed in Table 1.

Table 1. Synthesis routes of various inorganic nanotubes.<sup>7</sup>

Chalcogenide	Synthesis Route
WS <sub>2</sub>	(i) Heating MoO <sub>3</sub> in the presence of forming gas followed by heating in H <sub>2</sub> S (ii) WS <sub>3</sub> and (NH <sub>4</sub> ) <sub>2</sub> WS <sub>4</sub> decomposition in H <sub>2</sub> (iii) Pyrolysis of H <sub>2</sub> S/N <sub>2</sub> over WO <sub>3</sub> -coated MWNTs (iv) Laser ablation of WS <sub>2</sub> target
MoS <sub>2</sub>	(i) Heating MoO <sub>3</sub> in the presence of forming gas followed by heating H <sub>2</sub> S (ii) Decomposition of (NH <sub>4</sub> ) <sub>2</sub> MoS <sub>4</sub> in the pores of anodic alumina (iii) Decomposition of (NH <sub>4</sub> ) <sub>2</sub> MoS <sub>4</sub> MoS <sub>3</sub> in H <sub>2</sub> (iv) Hydrothermal treatment of ammonium thiomolybdate with ethylenediamine (v) MoS <sub>2</sub> powder covered with Mo foil, heated to 1300°C in H <sub>2</sub> S (vi) Laser ablation of MoS <sub>2</sub> target
MoSe <sub>2</sub>	(i) MoO <sub>3</sub> _ H <sub>2</sub> Se (ii) MoSe <sub>3</sub> and (NH <sub>4</sub> ) <sub>2</sub> MoSe <sub>4</sub> decomposition in H <sub>2</sub>
Nb–W–S	Heating Nb <sub>2</sub> O <sub>5</sub> coated W <sub>18</sub> O <sub>49</sub> nanorods in H <sub>2</sub> S at 1100°C
Mo–Ti–S	Pyrolysis of H <sub>2</sub> S/N <sub>2</sub> mixture over Ti–Mo alloy at elevated temperatures
NbS <sub>2</sub>	i) NbS <sub>3</sub> decomposition ii) CNT templated reaction
TaS <sub>2</sub>	TaS <sub>3</sub> decomposition
HfS <sub>2</sub>	Decomposition of HfS <sub>3</sub>
ZrS <sub>2</sub>	Decomposition of ZrS <sub>3</sub>
NbSe <sub>2</sub>	i) NbSe <sub>3</sub> decomposition ii) Electron irradiation of NbSe <sub>2</sub>
CdS, CdSe	Surfactant-assisted synthesis
ZnS	Sulfidization of ZnO columns by H <sub>2</sub> S at 400 followed by etching the core
NiS	Treatment of Ni(NH <sub>3</sub> ) <sub>4</sub> <sup>2+</sup> complex with CS <sub>2</sub> in aqueous ammonia
Cu <sub>5.5</sub> FeS <sub>6.5</sub>	Hydrothermal reaction between Cu and S in presence of LiOH.H <sub>2</sub> O and trace

Metal oxide nanotubes have been prepared by using a variety of techniques such as template reactions, sol-gel chemistry and hydrothermal methods. Anodic alumina pores have been used as templates for the growth of SiO<sub>2</sub>, TiO<sub>2</sub> and Al<sub>2</sub>O<sub>3</sub> nanotubes.<sup>7</sup>

## 2.3 Silica Nanotubes using template synthesis

Template synthesis of nanotubes from porous membranes, mainly anodic alumina pores, was pioneered by Martin and co-workers in the mid-1980's and has been used by many researchers for making nanotubes.<sup>3-6</sup>

### 2.3.1 Silica

Silicon oxide or silica (-SiO<sub>2</sub>)<sub>n</sub> is composed of the two most abundant elements in the earth's crust. Silicates make up a vast number of minerals and silica is present in glass and sand. Amorphous and crystalline silica possesses a hydrophilic surface due to terminal hydroxyl groups.. The optical transparency of silica in the visible wavelengths makes it amenable to spectroscopic studies Silica is also stable and compatible in biological environments.

### 2.3.2 Template Synthesis

Fabrication of useful nano materials for various applications is done using techniques including e-beam lithography, cluster method, and interference lithography. Nanotubes have been grown as thin films on the walls of cylindrical membrane pores using planar thin film techniques. One successful method for producing nanotubes is by template synthesis in nanoporous membranes. Template synthesis of nanotubes is achieved by

using different strategies such as electrochemical deposition, electro-less deposition, polymerization, sol-gel deposition, or chemical vapor deposition (CVD) in the nanoporous templates.<sup>4, 6-16</sup> When the pores are filled with the precursor solution it results in the formation of a self-assembled nano-array. Polycarbonate membranes and nanoporous alumina membranes are two widely used membranes. Aluminum oxide membranes consist of nanosized cylindrical holes perpendicular to the surface of the film. The membranes are available commercially in some fixed sizes with specific pore diameters or can also be prepared in the laboratory using electrochemical means.<sup>17</sup> Free standing nanotubes of any materials such as  $\text{TiO}_2$ ,  $\text{WO}_3$ ,  $\text{ZnO}_2$ ,  $\text{MnO}$ ,  $\text{SiO}_2$  can be obtained by template synthesis using anodic aluminum oxide membranes. This is achieved by dipping the membrane in a precursor sol after which gelation occurs. Concentration and viscosity of the initial sol and the immersion time can be varied to obtain nanotubes with desired wall thickness.<sup>11</sup> Sol-gel template synthesis has also been used to synthesize semiconductor oxide micro- and nanostructures within the pores of micro- and nanoporous membranes.<sup>18-20</sup>  $\text{TiO}_2$  nano-tubules and nano-fibers of the anatase form and other semiconductor oxides such as  $\text{MnO}_2$ ,  $\text{Co}_3\text{O}_4$ ,  $\text{ZnO}$ , have also been prepared.

### *2.3.3 Sol-gel process*

In this thesis we make use of the sol-gel process which is a method for preparing specialty metal oxide glasses and ceramics. Here we will deal specifically with sol-gel methods for the preparation of silica. In general, a single chemical precursor or a mixture of chemical precursors are hydrolyzed in solution to produce a gel state and finally

dehydrated to obtain a glass or ceramic. The sol-gel process has been developed extensively since 1980 and now it encompasses techniques to prepare fibers, microspheres, thin films, nano scale particles and tubes.

#### *2.3.4 Template Surface Sol-Gel (SSG) synthesis*

The Surface Sol Gel (SSG) method<sup>15</sup> illustrated in Figure 3 involves repeated cycles of the two step deposition cycles in which the adsorption of a molecular precursor and the hydrolysis are followed by a post-adsorption wash. The washing steps aid in removing weakly bound molecules and prevent formation of additional non-uniform layers. This approach allows finer control of wall thickness than conventional sol-dipping techniques and each adsorption/hydrolysis cycle results in only one layer. SSG is a flexible method to produce nanotube membranes and free standing single nanotubes. The thickness and the porosity of the tubes can be precisely controlled by changing the composition of the precursor solution and the number of deposition cycles. Using 100-mol%  $\text{SiCl}_4$  precursor we can obtain nanotubes with wall thickness of  $\sim 15$  nm in approximately 15 deposition cycles. The number of cycles varies depending on relative humidity and perhaps other operating conditions that remain undefined.

In the layer by layer template synthesis of hydrophobic silica nanotubes carbon-tetrachloride may be replaced by hexane. In addition to switching to hexane, several other washing cycles involving mixtures of hexane-methanol and pure ethanol has been introduced to obtain colloidal nanotubes with uniform and predictable wall thickness.

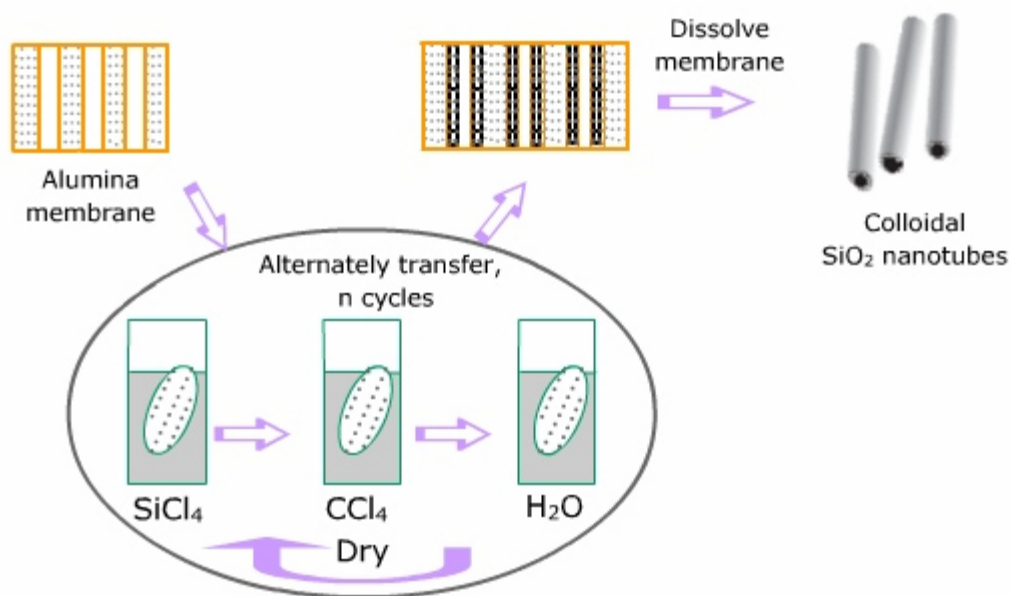
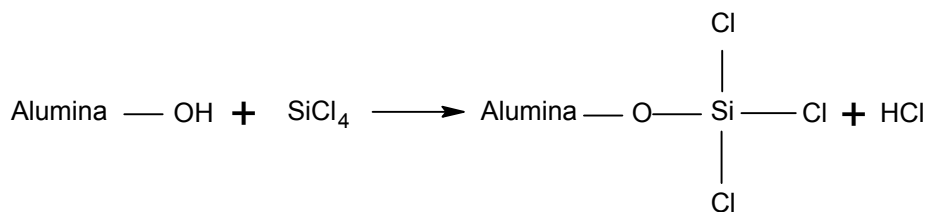


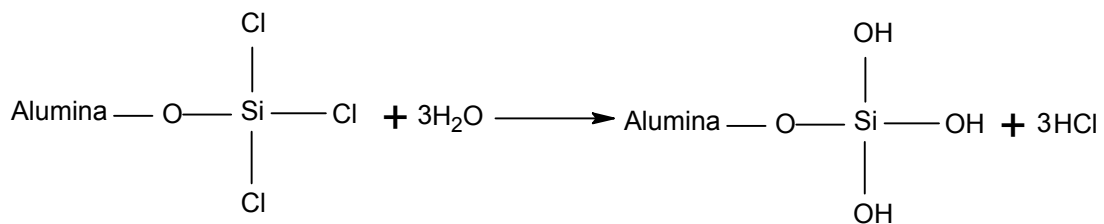
Figure 3. Surface Sol-Gel synthesis of Silica Nanotubes.<sup>15</sup>

The surface reactions during the SSG synthesis are described below:

1. Reaction of the  $-\text{OH}$  groups on the alumina surface with  $\text{SiCl}_4$  (membrane immersion in  $\text{SiCl}_4$ ).

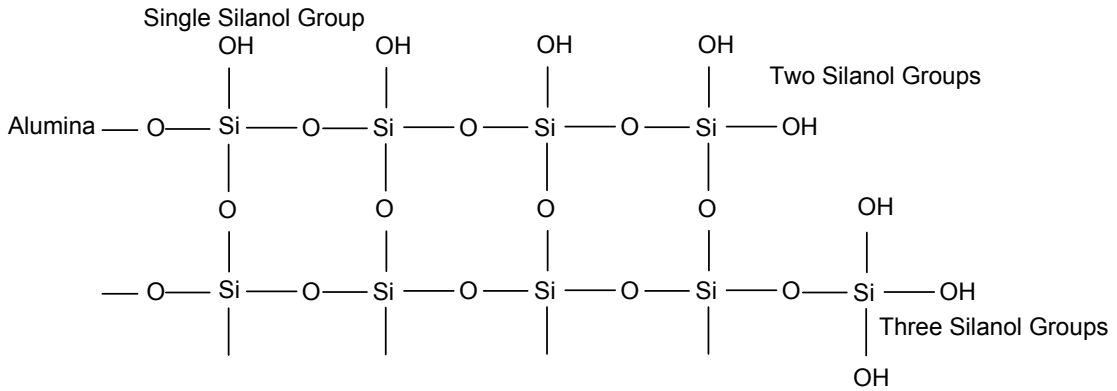


2. Reaction of the chlorinated silanes with water (washing in DI water)

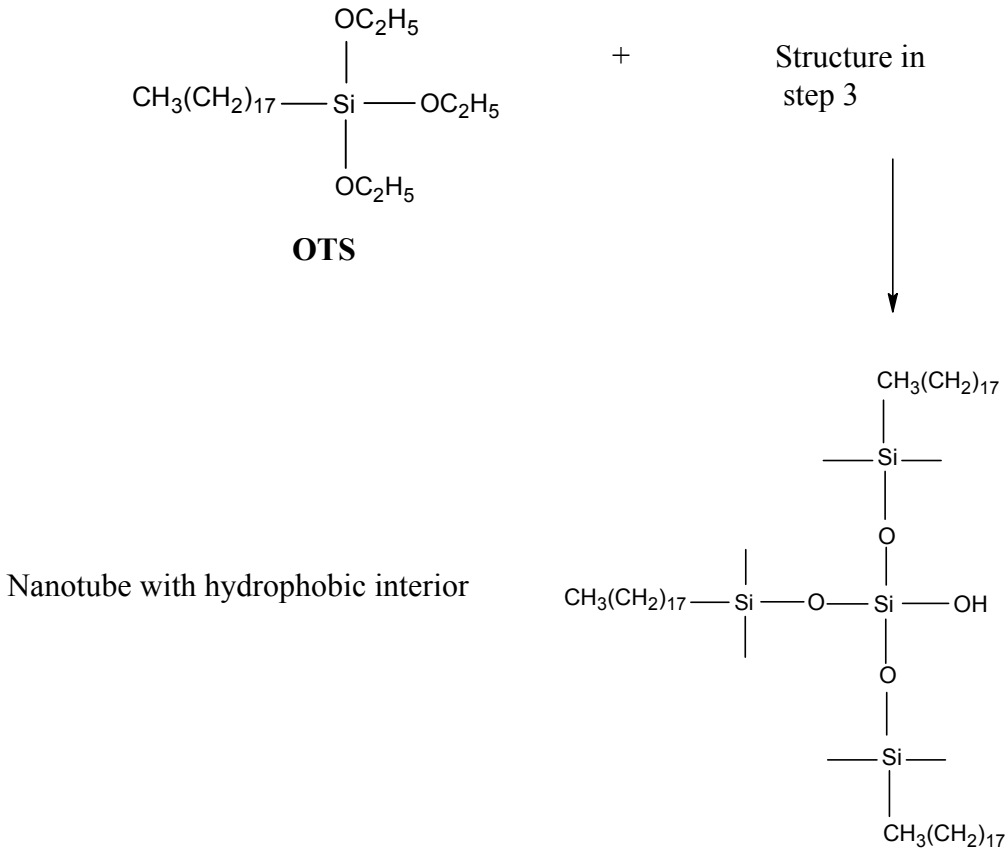




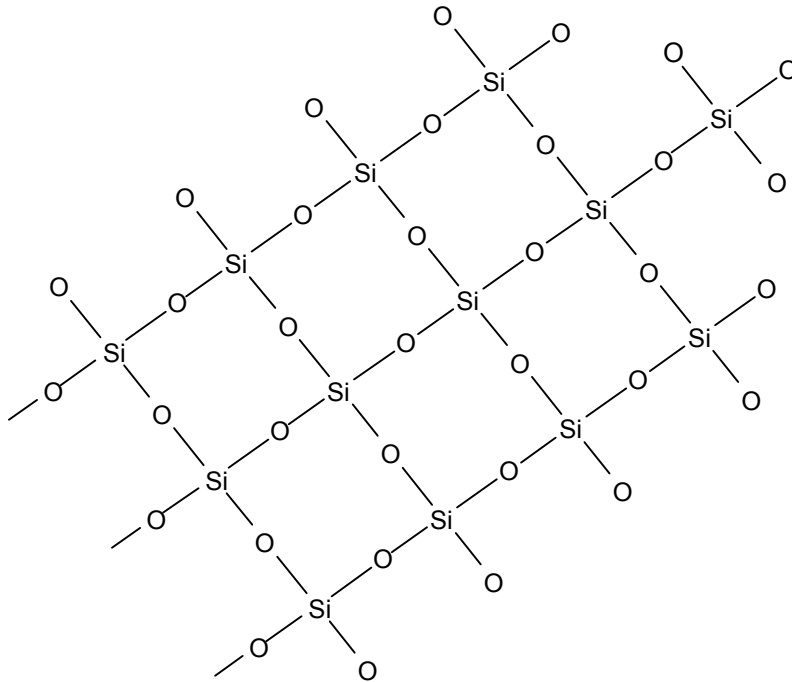
3. Formation of silanol groups after several deposition cycles (cross linking with the several –OH groups on the alumina membrane)



4. After the desired deposition cycles, the membrane is treated with OTS (octadecyltrimethoxysilane) to make the interior of the membrane hydrophobic.



5. The membrane is baked at 120<sup>0</sup>C and alumina membrane is removed by chemical and/or mechanical polishing to obtain colloidal SiO<sub>2</sub> nanotubes. Below is the SiO<sub>2</sub> structure.



Sol-gel template synthesis has the following unique advantages<sup>3, 4, 16, 21</sup>:

- Nanotubes have open ends and has distinct inner and outer surfaces (hydrophobic, hydrophilic, positively or negatively charged)
- The inner voids can be filled with various chemicals or materials such as fluorescence dyes, drug molecules, biomolecules, and nanoparticles both during and after synthesis.
- Nanotubes can be synthesized out of many materials such as silica, gold, titanium or cadmium.
- Inner/outer diameters, length, tube wall thickness, can be easily tailored to fit the application.

### *2.3.5 Applications of template synthesized nanotubes*

Template synthesized metal nanotubes can be used for chemical separations.<sup>16,21,22</sup> Nanotubes made out of conducting polymer( PEDOT)<sup>6</sup> (who cares about this? You should really only focus on silica and the areas you worked on) show promise for use in fast-response electro chromic displays.<sup>6</sup> Silica nanotubes can be used for bio separations bio-molecular storage and delivery.<sup>4,21,23</sup> Silica nanotubes with magnetite particles inside them can be used for magnetic filed assisted separations, bio interactions and drug delivery.<sup>10,24</sup> Nanotube – based DNA sensing is gaining increased attention and DNA – functionalized nanotubes can be used as gene delivery vehicles.<sup>25</sup> Silica nanotubes can be employed as nanoreactors or miniature reaction vessels to understand or mimic biological reactions. Understanding transport in silica nanotubes will lead to developing nanofluidic devices to carry out bio separations.

## 2.4 Nanotube Characterization

Powerful analytical techniques, namely transmission electron microscopy (TEM) and scanning electron microscopy (SEM), are used to study and characterize nanomaterials. In scanning electron microscope (SEM) electrons from a metal filament are collected and focused into a narrow beam which scans across the target (ex: nanotube), synchronized with a spot on a computer screen. Electrons scattered from the nanotube are detected and current is produced which makes the spot on the computer brighter or darker. This creates a photograph-like image with an exceptional depth of field. Magnifications of several thousand times are possible. Transmission electron microscope (TEM) is capable of magnifications of 100,000 times and extreme resolution. TEM uses electrons passing

through a very thin slice of the specimen and magnetic lenses focus the electron beam, and project the highly-magnified image onto a phosphor screen or special photographic film.<sup>26</sup> SEM and TEM images of nanotubes synthesized by various researchers are illustrated in Figure 4. Figure 4 (A) reveals the cross-sectional view of nanotube arrays, (B) reveals the wall thickness achieved by template synthesis, (C) shows multilayered gold nanoparticles nanotubes. (D) shows the internal morphology of polymer nanotubes. These images showcase that electron microscopy techniques can provide valuable information about nanomaterials including but not limited to structure or morphology, size and wall thickness and electron microscopy techniques are powerful and indispensable.

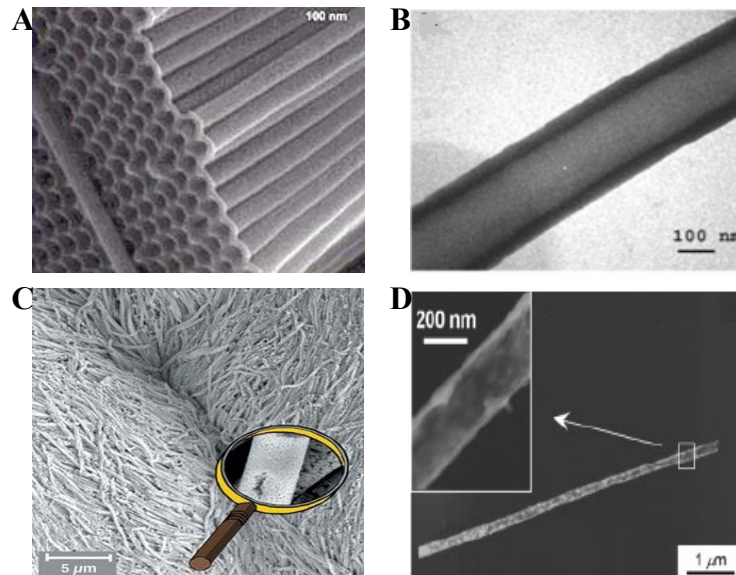


Figure 4. Electron micrographs : (A) SEM image of CVD template synthesized nanotubes.<sup>8</sup> (B) TEM image of a SiO<sub>2</sub> nanotube.<sup>15</sup> (C) SEM image of gold nanoparticles nanotubes.<sup>12</sup> (D) TEM image of a PEDOT nanotube<sup>6, 27</sup>.

## 2.5 Laser Scanning Confocal Fluorescence Microscopy

With the invention and development of lasers as ideal single beam light sources, laser scanning confocal microscopy evolved as a standard technique and it employs a pair of pinhole apertures to limit the specimen focal plane to a confined volume approximately a micron in size. Laser scanning confocal microscopy depends on fluorescence and hence a sample needs to be treated with trace amount of fluorescent dyes to make things visible. Lasers are high intensity monochromatic light sources and are widely used for various techniques such as lifetime imaging studies, photobleaching recovery, and total internal reflection fluorescence.<sup>28</sup>

### *2.5.1 Confocal Microscopy*

The principle of confocal microscopy was developed by Marvin Minsky in 1953. Advantages of confocal microscopy include controllable depth of field, imaging optical sections from thick specimen and imaging without out-of-focus problems. Spatial filtering is employed to eliminate out-of-focus light in samples that are thicker than the plane of focus. In any microscope the highest intensity of the excitation light is at the focal point of the lens, however fluorescence originating from regions above or below the focal plane leads to haze in the image. Adding a pinhole allows the focal point of the objective lens of the microscope to form an image where the pinhole is. The pinhole is conjugate to the focal point of the lens and hence it is confocal pinhole.

### *2.5.2 Fluorescence Microscopy*

When we shine light on some molecules we will see light of a different color emitted from those molecules and this phenomenon is referred to as fluorescence. The color of the light emitted and the excitation light wavelength depends on the material. A fluorescence microscope uses a special dichroic mirror that reflects light shorter than a certain wavelength and transmits only light longer than that wavelength. Epi-fluorescence is a particular style of fluorescence microscopy where the microscope objective is used to illuminate the sample. The main advantage of fluorescence microscopy is that fluorescent dye molecules can be tagged to specific sample surfaces and they can be studied under the fluorescence microscope

## 2.6 Fluorescence Recovery After Photo Bleaching

Photo-bleaching can be considered as photo induced alteration of a fluorophore that extinguishes its fluorescence. Fluorescence recovery after photobleaching (FRAP) was developed in the 1970's as a technique to study the mobility of proteins in living cells by measuring the rate of recovery of fluorescence signal at the bleached site.<sup>29</sup> It was initially designed by Axelrod and coworkers to measure two-dimensional diffusion of membrane-bound molecules. With the advancement of confocal scanning microscope and introduction of Green Fluorescent Protein (GFP), the FRAP technique gained renaissance and has been increasingly used since then.<sup>30</sup> In this technique, a region in the sample is selectively bleached with a high intensity laser and the recovery that occurs as other unbleached molecules move into that region is monitored over time with low intensity laser light. Analysis of recovery can be used to determine diffusion constant, transport

rate and other kinetic parameters of a protein or any other fluorescent molecules. For accurate analysis of FRAP data, bleach time must be much shorter than the recovery time.

FRAP techniques have been widely developed for use on laser scanning confocal microscope. Acousto-optical tunable filters are used to allow rapid switching between the bleaching and normal beam, resulting in accurate measurements. Figure 5 illustrates a typical recovery curve. Table 2 list some of the FRAP considerations applicable when analyzing samples, with example based on biological specimens.

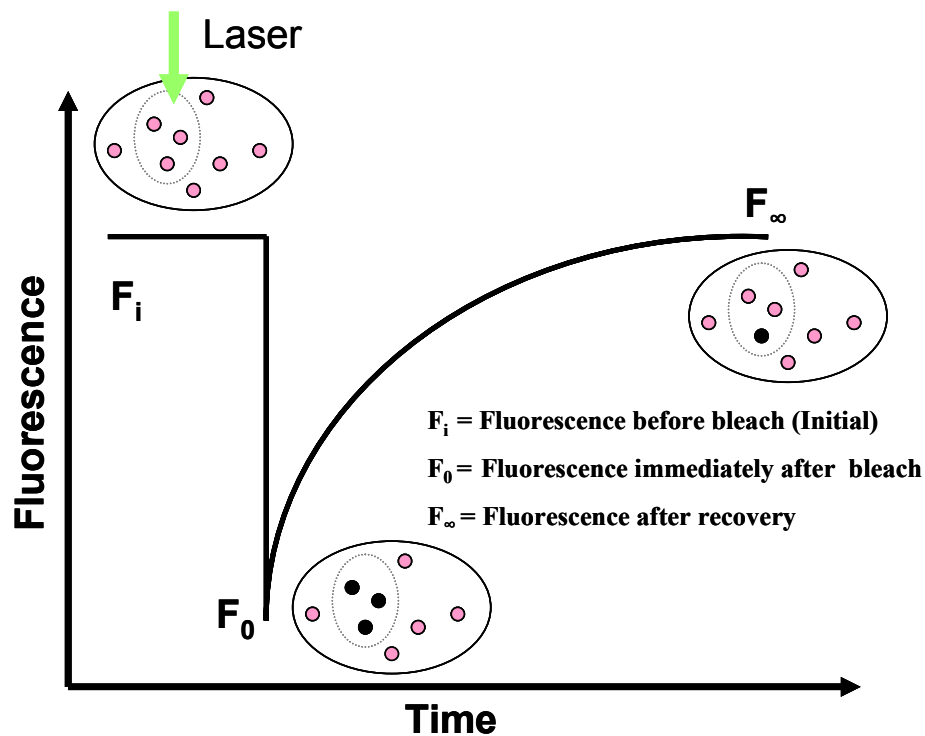


Figure 5. Illustration of Fluorescence Recovery After Photobleaching .

Table 2. Fluorescence Recovery After Photobleaching Considerations.<sup>adapted</sup>  
 from 30

Problem	Potential explanations
Lack of recovery or partial recovery after photo bleach	Possible explanations include: an immobile fraction of unbleached molecules that could not diffuse into the bleached region; an immobile fraction of molecules in the bleached area that was unable to exchange with the incoming unbleached molecules; or the bleached area is not continuous with the rest of the cell (for example, a separate membrane compartment).
Reversible photobleaching of GFP	The excitation might cause the GFP molecule to flicker or to be sequestered in a triplet state. Both of these situations can result in the recovery of fluorescence (in milliseconds to several seconds) of the GFP molecule in the absence of diffusion. To control for any reversible photobleaching of the GFP in a FRAP experiment, the FRAP conditions should be repeated in fixed samples in which no recovery of fluorescence should be expected. Or, alternatively, the bleach spot size could be varied and the changes in the timescale of recovery could be confirmed.
Non-diffusive Behavior	Measurements in FRAP studies are often complicated by the binding and dissociation of fluorescent molecules to and from intracellular components. This is usually reflected in the FRAP curves by longer recovery times, by an incomplete recovery (an immobile fraction) or by the presence of several slopes (indicating several recovery processes over different timescales). Kinetic modeling methods, along with computer simulations, have been useful tools to dissect and analyze the recovery curves obtained by



Problem	Potential explanations
	FRAP. A kinetic model is characterized by biophysical parameters, such as binding and release rate constants, diffusion constants, flow rates and residence times. The model can be simulated on the computer for different parameter values. Once the parameters that best fit the experimental data have been determined, the predictions of the model can be tested experimentally.
D values of the same ROI in the same cell in two consecutive experiments are different	A potential explanation is damage to the photo bleached area. Decreasing the bleach time, acquisition time or the excitation beam intensity during the recovery period could avoid damaging the cell. Using YFP rather than GFP or CFP will also make it easier to photo bleach.

*CFP, cyan fluorescent protein; ROI, region of interest; YFP, yellow fluorescent protein.*

Predominantly FRAP is being used for understanding the diffusion and transport properties in biological samples. For the first time FRAP has been extended to understand diffusion and transport properties of silica nanotubes.<sup>31</sup>

## 2.7 Solvatochromism

Solvatochromic dyes change color according to the polarity of the liquid in which they are dissolved. Reichardt's betaine dye, pyrene, dansylamide, Nile Red and 1-pyrenecarbaldehyde are some example of solvatochromic dyes. Due to interplay of

various interactions in any solvent-solute system it is very difficult to define polarity on an absolute scale. It is possible to effectively gauge the relative polarity of a particular solvent with different solutes or interface or attached functional groups.

Nile red is a phenoxazone dye that fluoresces intensely in varying color, in organic solvents and hydrophobic lipids. The dye acts as a fluorescent hydrophobic probe as its fluorescence is mostly quenched in water.<sup>32</sup> Nile Red is a positive solvatochromic dye and it exhibits a  $\lambda_{\text{max}}^{\text{ex}}$  of 484 nm and  $\lambda_{\text{max}}^{\text{em}}$  of 529 nm in non-polar solvents and  $\lambda_{\text{max}}^{\text{ex}}$  of 591nm and  $\lambda_{\text{max}}^{\text{em}}$  of 657 nm in polar solvents. As polarity of the medium surrounding increases, absorption, excitation and emission maxima of Nile Red shift to lower energies. Figure 6 shows the emission spectra of Nile red in various solvents.

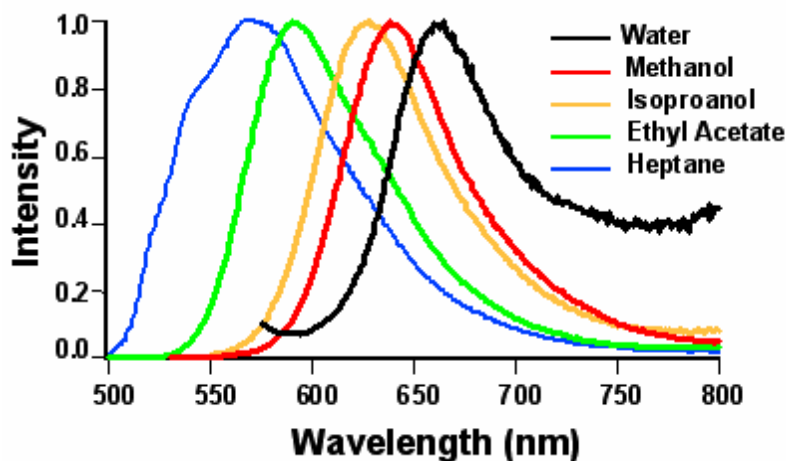


Figure 6. Fluorescence emission spectra of Nile red in various solvents. For the spectrum in water a small proportion (2%) of methanol was added to aid dissolution.

## 2.8 Wetting and Capillarity

Surface properties of nanoporous materials and their interactions with liquid are fundamental in developing nanoreactors and nanofluidics devices and hence an understanding of the wettability of nanostructures is important.

### *2.8.1 Contact angle and surface tension*

Whenever a solid surface is being wetted by a liquid, the angle formed by the liquid at the intersection of solid, liquid and vapor phase is denoted as contact angle ( $\theta$ ).<sup>33, 34</sup>

When the liquid completely spreads on the solid surface,  $\theta$  is zero. If the angle  $\theta$  is less than  $90^\circ$  the liquid wets the surface and if the angle  $\theta$  is greater than  $90^\circ$ , the liquid is said to be non-wetting. Figure 7 describe the extent of wetting at various contact angles.

At any fluid-fluid interface, there exist forces arising out of the interactions between the molecules. This excess surface energy is measured in dynes/cm or mN/m and referred to as surface tension or interfacial tension, if the interface is liquid- vapor or liquid-liquid respectively. Water being polar has strong intermolecular interactions and hence high surface tension. Adding surfactants, adding solvents with lesser polarity, increasing the temperature will reduce the intermolecular interactions and hence lowers the surface tension of water.<sup>35</sup>

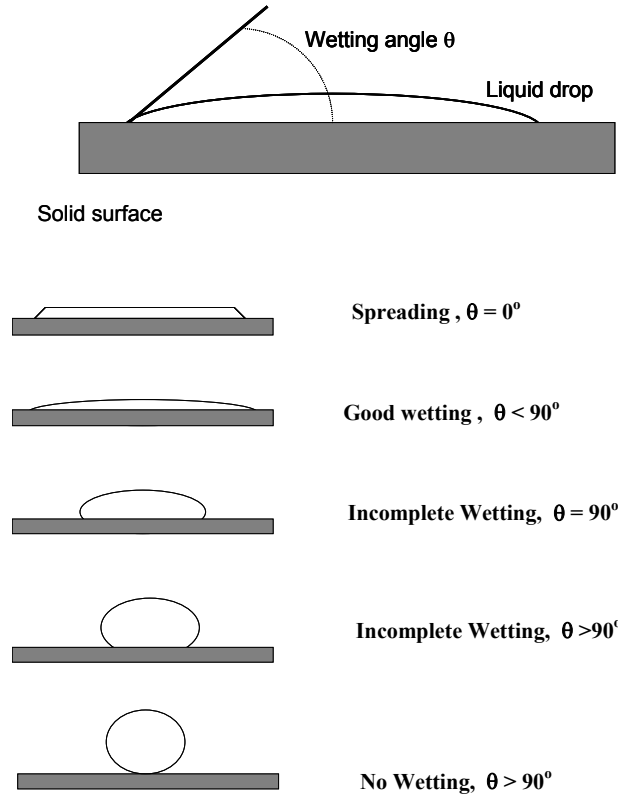


Figure 7. Contact angles and extent of wettability.

### 2.8.2 Laplace equation and capillarity

Knowing the general wetting phenomena of macroscopic systems can aid in understanding the wetting of nanotube interiors. When a liquid wets a capillary we have the Laplace equation

$$\Delta P = \frac{2(\gamma_{SV} - \gamma_{SL})}{r} \quad (1)$$

Here  $\Delta P$  is the pressure causing a liquid to fill a capillary,  $\gamma_{SV}$  and  $\gamma_{SL}$  are the free energy per unit area of solid- vapor and solid – liquid interfaces respectively. From the contact angle measurements and using Young’s equation we could obtain the difference ( $\gamma_{SV} - \gamma_{SL}$ ). Young’s equation is given as

$$\gamma_{SV} - \gamma_{SL} = \gamma_{LV} \cos \theta \quad (2)$$

where  $\gamma_{LV}$  is the surface tension of the liquid, and  $\theta$  is the contact angle at vapor/liquid/solid interface.  $\cos \theta$  is known as wetting coefficient with a positive value indicating wetting will occur and negative value indicating absence of wetting. Contact angle measurements were done for each solvent on a hydrophobically modified planar surface ( $C_{18}$  coated coverslip). The Young- and Young-Laplace equations accurately describe the wetting of plane surfaces by liquid drops and the rise or depression of liquids in glass capillaries.<sup>31,33</sup> Figure 8 illustrates capillary rise in water and capillary depression in mercury. Combining equation 1 and 2 we have the Young-Laplace equation which is given as

$$\Delta P = \frac{2 \gamma_{LV} \cos \theta}{r} \quad (3)$$

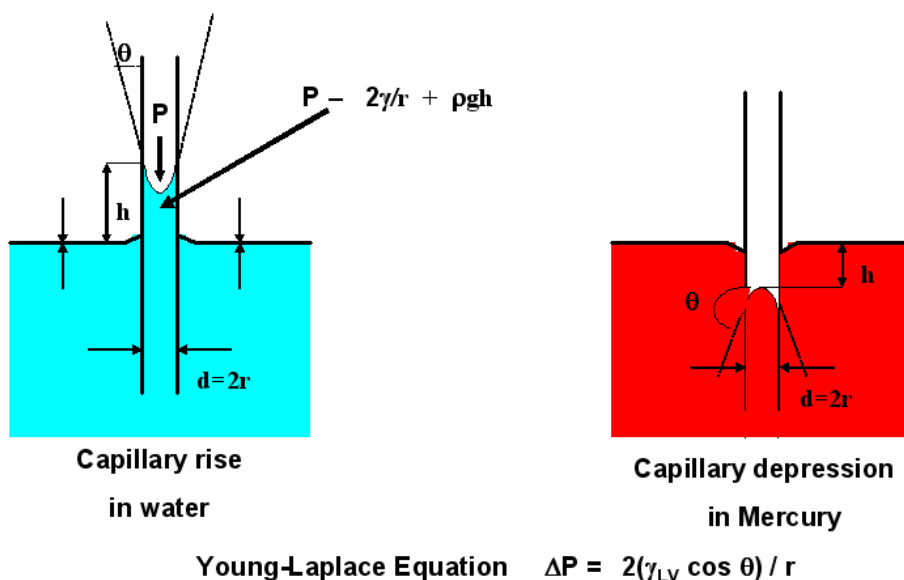


Figure 8. Laplace equation and capillarity phenomena (capillary rise in water and depression in mercury).

### *2.8.3 Nanoscale Capillarity*

The nanotubes in this study will be treated as nanocapillaries and using Young-Laplace equation, pressure differences can be estimated at the curved interface. Experimental results for the wettability of nanotubes can be compared with these pressure estimates and we can answer the questions “Does the classical capillary theory describe the wetting at nanoscale?” A recent study by Fadeev and coworkers has shown that the Young-Laplace underestimates capillary pressure by as much as a factor of 2 for water in hydrophobic pores of a few nanometers.<sup>36</sup> At nanoscale, there will be other interesting but yet unclear phenomena such as capillary condensation, evaporation, spontaneous drying.

## 2.9 Hydrophobic Effects or Interactions

Hydrophobic effect is the tendency of non-polar groups to cluster so as to shield them from contact with aqueous environments. Water-induced attraction between non-polar molecules is called the hydrophobic interaction. The role of hydrophobic effect is to maintain stability of mesoscopic assembly and biological structure in aqueous environments. Hydrophobic phenomena in structural biology related to forces in the interpretation of protein denaturation were appreciated by Kauzmann.W in 1959. Existence of a crossover from small to large length scale hydrophobicity was appreciated by Stillinger F.H in 1973. Bubbles with radii larger than 1nm gets subjected to dewetting or drying. Pratt-Chandler theory (1977) states that molecular density fluctuations in water at small length scales obey Gaussian statistics. Liquid water surrounding a small

hydrophobic molecule is different than the bulk water. Anders Wallqvist and Bruce Berne verified that dewetting occurs between two nano-scale hydrophobic plates immersed in water.<sup>37</sup> Neither extreme of a small length scale or a large length scale is sufficient to explain hydrophobicity. Hydrophobicity treatment must describe both regimes simultaneously. Lum-Chandler-Weeks (LCW) molecular theory of crossover was proposed in 1999 and it states that crossover occurs on nanometer length scales when apolar concentration is high and apolar surface is sufficiently large. LCW theory has implications on : (i) Kinetics of dewetting between macroscopic plates , (ii) Temperature dependence of protein folding,(iii) Solvation and assembly of nano-scale cylinders.<sup>38-45</sup>

### *2.9.1 Length scale hydrophobic effects*

The length scale dependent hydrophobic effects (changes in hydrophobic effect with changes in length scale) is one area in the subject of hydrophobicity which is still dealt with uncertainty as it lacks extensive experimental observations. As early as 1973 existence of a cross over from small to large length scale was observed. The prediction that crossover might occur at nanoscale regime was confirmed by observing de-wetting between two nanoscale hydrophobic plates immersed in liquid.<sup>39</sup> Later a general molecular theory of the crossover called Lum- Chandler-weeks theory was developed.<sup>42</sup> According to the theory, liquid water when confined between extended hydrophobic plates, exist in its meta-stable state provided drying occurs when surfaces are close. There exists a thermodynamic instability for the vapor phase of water at any separation distance of 100nm between two parallel plates.<sup>46,43</sup> Figure 9 demonstrates the contrast between small and large length scale hydrophobicity. In other words theory predicts that long

range hydrophobic effects can destabilize liquid water between extended hydrophobic surfaces which are separated by less than the critical distance  $d_c$  as given by the relation

$$d_c \approx \frac{2\gamma}{n_l(\mu_l - \mu_g)} \quad (4)$$

where  $\gamma$  is the constant of proportionality,  $n_l$  is the molecular density of bulk liquid,  $\mu_l$  is the chemical potential of liquid,  $\mu_g$  is the chemical potential of gas. At separations of 10-20 nm two hydrophobic plates jump into contact as observed during surface force measurements. This is due to the cavitation of the interstitial water.<sup>37</sup> Large surface tension of water and the small difference between liquid and gas potential accounts for the instability in the liquid phase.<sup>42</sup>

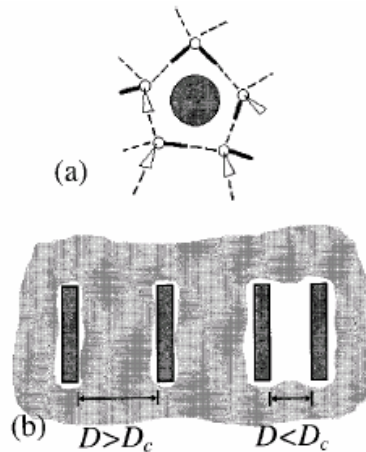


Figure 9. (A) Schematic view of local water structure near a small hydrophobic sphere. Dashed lines indicate hydrogen bonds. (B) Schematic view of water structure near large parallel hydrophobic plates. Shaded area indicates regions where water density is essentially that of the bulk liquid; vacant regions indicate where water density is essentially that of the bulk vapor. <sup>adapted from 42</sup>



### *2.9.2 Theoretical predictions on hydrophobic effect / Solvent confinement in hydrophobic environments*

Liquid – vapor coexistence should occur on a larger length scale in the nanotubes as observed in the studies done on water confined in cylindrical micropores.<sup>47, 48</sup> Giaya *et al* investigated the behavior of fluid in the confined cylindrical pores. Using the model of characterizing water-like fluids confined in pores, it has been shown that the density of the fluid inside pores is smaller than the bulk liquid density for small pores of hydrophobic materials. Also it predicts that the fluid density inside the pores approaches the bulk liquid density very quickly as the radius increases and or the hydrophobicity decreases.<sup>40, 47</sup> The model took into account the hydrogen bonding interaction, between fluid-fluid and fluid-pore-wall interactions. With pure water outside these nanotubes, the fluid inside these tubes should be vapor until the radius is ~1500nm and above this pore radius the fluid might exist in liquid state. It is to be noted that the critical radius after which the solvent changes from vapor to liquid inside a pore decreases as the fluid- wall interaction increases.

To quantify hydrophobic hydrations and interactions on a molecular scale a theoretical approach has been developed and this model relates the probability for cavity formation in bulk water and the hydration free energy of the hydrophobic solutes.<sup>40</sup> The probability is estimated using an Information Theory (IT) approach and this IT approach provides a simple theoretical framework to study many hydrophobic phenomena on a molecular scale. The temperature dependence of hydrophobic hydration and pressure denaturation of proteins can be well understood.

Recent attraction in theoretical studies is the problem of water confinement in pores on the nanometer scale. The free energy of a hydrophobic tube could be very close to that of the empty tube as demonstrated by the molecular dynamics study of water penetration of a nanotube.<sup>41</sup> Also a lattice model of water confined in hydrophobic nanotubes was studied and it was shown that the filled and the empty tube could be energetically degenerated corresponding to two separate minima in the free energy distribution function. Emptying of a filled tube is associated with a large entropic barrier while the filling of an empty tube is associated with a large energetic barrier.<sup>44</sup>

Hydrophobic interaction would not occur without an aqueous environment. Liquid water is held together by random fluctuating three-dimensional network of hydrogen bonds and this structure is responsible for the various behaviors of water. Attraction between hydrophobic surfaces in water is the reason for the protein folding stability. For a small solute the number of water molecules that get affected by the solute is proportional to the solute volume and hence the solvation free energy. For extended hydrophobic surfaces, the free energy of a solute is proportional to the surface area of the interface between solute and water. The answer for the questions whether the depleted water would be really gas-like or ice-like is till unclear. A recent simulation shows that the depleted water is more ice-like inside a hydrophobic carbon.<sup>38,39</sup>

In the process of studying the filling and emptying kinetics of carbon nanotubes in water by molecular dynamics simulations it was observed that filling thermodynamics and kinetics depend sensitively on the strength of attractive – water – nanotube interactions and this sensitivity increases with the length of the tubes.<sup>45</sup>

## Chapter 3: Experimental details

### 3.1 Synthesis of Silica Nanotubes

Silica nanotubes with 170 and 30 nm i.d. and lengths 10-15  $\mu\text{m}$  were synthesized using layer-by-layer template synthesis. Commercially available alumina templates were used to synthesize 170 nm tubes and templates for synthesizing 30 nm tubes were fabricated in-house. To synthesize 170nm tubes, anopore aluminum oxide membrane with pore diameter of 0.2  $\mu\text{m}$  and thickness of 60  $\mu\text{m}$  was used. The anopore have high pore density and narrow pore size distribution. Fabrication procedure of the template for 30 nm tubes is not a main part of this work and the procedure is detailed elsewhere.<sup>17,49</sup> Briefly hexagonally ordered pore arrays were obtained by anodizing degreased, cleaned and annealed aluminum under constant potential in phosphoric acid solution. There exists a linear relationship between the pore distance and the anodic voltage. Figure 10 shows the top view (A) and cross-sectional view (B) of the alumina template synthesized in house.

The SSG procedure detailed previously<sup>13,15,21</sup> was used to obtain silica nanotube membranes. Wall thicknesses of 2-15 nm can be obtained by varying the deposition cycles in the SSG synthesis. Nanotubes with hydrophobic interior surface were produced by immersing the silica-coated surfaces in a solution of 5% (v/v) octadecyltrimethoxysilane and 16 mM acetic acid in ethanol/water (95% v/v) for 30 min. at room temperature followed by rinsing with ethanol and curing at 150  $^{\circ}\text{C}$  for 2 h. Table 3 explains the various adsorption – deposition cycles involved in the template surface sol-gel synthesis of silica nanotube membranes with 170 nm and 30 nm inner diameter. The

intact silica nanotube membrane with hydrophobic interior surface was used for the membrane transport measurements.

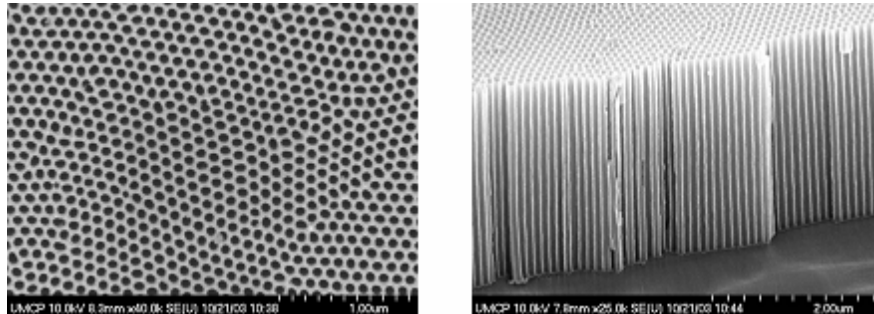


Figure 10. Alumina templates with pore diameter of 60nm (A) Top view (B) Cross-sectional view).

The procedure for template synthesis of silica nanotubes is schematically shown in figure 11. To obtain free standing nanotubes from the membrane, both faces of the sol-gel treated template membrane were mechanically polished to remove the silica surface layers and expose the underlying template alumina.

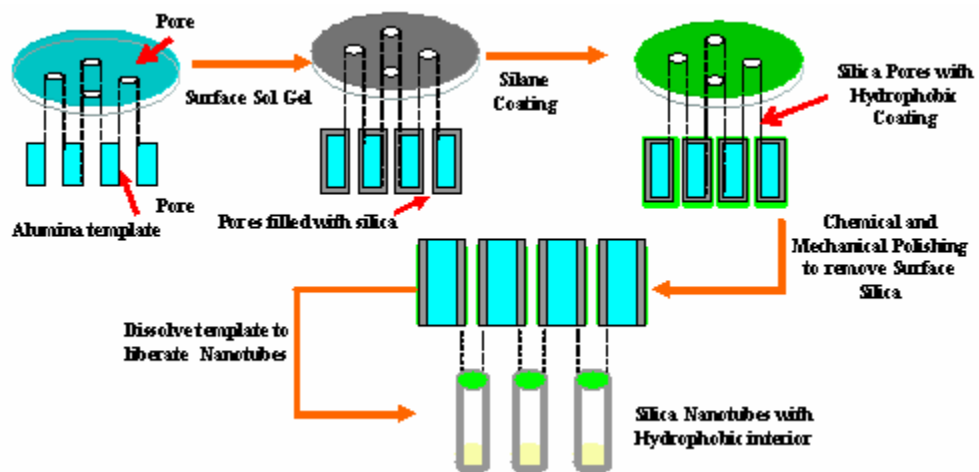


Figure 11. Schematic of sol-gel template synthesis of silica nanotubes.

Chemical polishing of both the surfaces with mild hydrofluoric acid can also be followed. The template was then dissolved by immersing the membranes overnight in a 25% (wt/wt) aqueous solution of  $H_3PO_4$ . The liberated nanotubes are then filtered from the acid solution and repeatedly rinsed with deionized water. <sup>15, 17, 18, 49, 50</sup>

Table 3. Steps involved in sol-gel template synthesis of silica nanotube membranes.

No	Description	Duration
1	Remove the polypropylene support ring around the Whatman Anopore membrane	N/A
2.	Immerse the membrane(s) in acetone and sonicate	10 minutes
3.	Treat the membranes with 25% $HNO_3$	1 minute
4.	Rinse with purified water	until pH ~ 7
5.	Air dry the membrane(s)	~10 minutes
6.	Immerse the membranes in $SiCl_4$	2 minutes
7.	Immerse the membranes in hexane (1 <sup>st</sup> wash)	10 seconds
8.	Immerse the membranes in hexane (2 <sup>nd</sup> wash)	10 seconds
8.	Immerse the membranes in hexane (3 <sup>rd</sup> wash in fresh hexane)	5 minutes
9.	Immerse the membranes in hexane : methanol (1:2)	5 minutes
10.	Immerse the membranes in ethanol	5 minutes
11.	Dry the membranes in $N_2$ stream	5 minutes
11.	Immerse the membranes in water	5 minutes
12.	Immerse the membranes in methanol	5 minutes
13.	Dry the membranes in $N_2$ stream	10 minutes

## 3.2 Single Nanotube measurements

### *3.2.1. Fluorophore adsorption*

Dye was introduced to the nanotube interior by immersion of nanotubes in a DiIC<sub>18</sub> or Nile red solution ( $10^{-7}$  M) of water/methanol (9:1 v/v). Sonication is used to disperse the nanotubes and to facilitate filling of the nanotube with the dye solution. Filling of the nanotubes did not occur without sonication. After sonication, the sample is centrifuged to concentrate the nanotubes. The supernatant is removed and nanotubes are suspended in deionized water. The sonication-centrifuge-rinse steps are repeated several times, after which the solution is diluted with deionized water and stored in the dark until needed. Figure 12 shows the schematic of the procedure for introducing dye to the nanotube interior. DiIC<sub>18</sub> has two hydrophobic tails and a charged indocarbocyanine head group and partitions well to the OTS interface in polar solvents. Nile red, which has been used as a sensitive probe of micro environments in sol-gel films<sup>51</sup>, is also sequestered in the hydrophobic nanotube interior when introduced using the procedure described above. Care was taken to use only trace amounts of these dyes, corresponding to an average of 1 dye molecule per 20 nm<sup>2</sup>, at concentrations which do not significantly alter the contact angle of the immersing solvent with the substrate.<sup>31</sup>

### *3.2.2 Sample Preparation for FRAP experiments:*

Cover slips are immersed in a 1:1:4 mixture of 1M HCl, tetraethoxysilane (TEOS) and ethanol, then sonicated for 5 minutes and finally rinsed with ethanol. TEOS promotes sol-gel processing thereby enabling immobilization of nanotubes. To achieve random distribution of immobilized nanotubes, TEOS coated cover slips are wetted with the

nanotubes solution and allowed to dry overnight at 25°C. A rubber spacer (o-ring) is placed around the sample spot in the cover slip which is then filled with the solvent of interest and sealed with a second plain clean cover slip to prevent evaporation. The nanotube coated cover slip forms the bottom surface. In addition to confocal imaging the microscope could be switched to the wide field; epi-illumination employing a color Charged-Coupled Device (CCD) camera and sample would be imaged quickly to find individual nanotubes for FRAP analysis.<sup>31</sup>

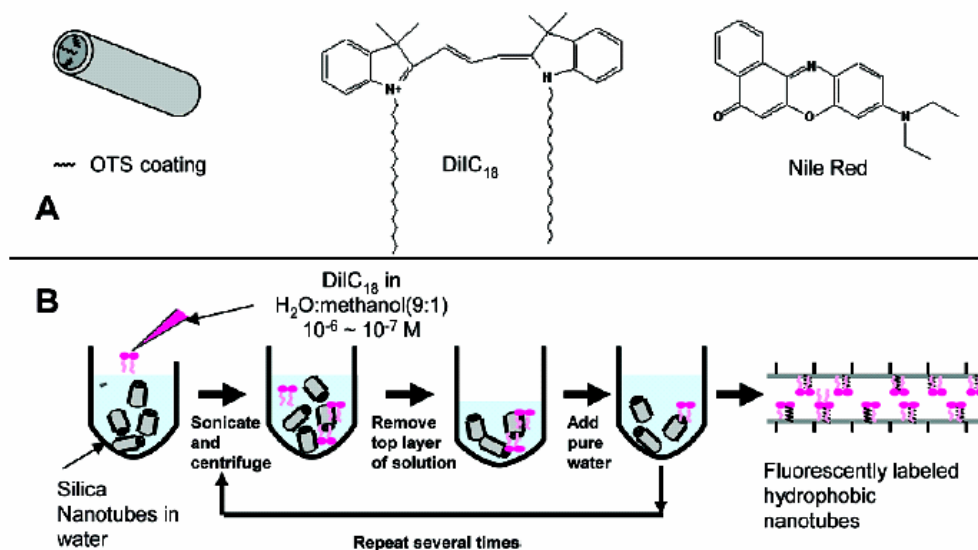


Figure 12. Introduction of dye to the OTS-modified hydrophobic nanotube interiors. (A) OTS-modified silica nanotubes were stained with either DiIC18 or Nile Red by physisorption to the hydrophobic interior surface. The surfactant-like fluorescent dye, DiIC18, was used in FRAP experiments, and the solvatochromic dye, Nile Red, was used as a reporter of local dielectric properties inside individual nanotubes. Both dyes partition well to the hydrophobic interface and only trace amounts were used to ensure that the nanotube's internal surface properties were not significantly altered by the

adsorbed dyes. (B) Step-by-step scheme showing the procedure for the introduction of DiIC18 to the nanotube interior. Nile red was introduced in an analogous manner.<sup>52</sup> Reproduced with permission from J. Am. Chem. Soc. 2005, Copyright 2005 Am. Chem. Soc.

### 3.2.3 FRAP Experiments

Using a focused laser spot, several points on the same nanotubes are bleached for a particular time (10 – 30 seconds). Dye molecules at the irradiated point gets photo bleached changing to a dark spot. Figure 13 is a cartoon description of FRAP in silica nanotubes. To monitor the recovery of fluorescence, laser intensity is reduced to four orders of magnitude after bleaching and a series of fluorescence images are obtained. Intensity obtained by analyzing the bleached area (using the series of fluorescence images) is plotted as a function of time to give a recovery curve for each bleached spot. Steps followed to conduct FRAP experiments are detailed in Appendix A.

Recovery curves are then analyzed by fitting with the following function:

$$I(t) = I(\infty) - G(t) \quad (5)$$

where  $I(\infty)$  is fully recovered intensity

and  $G(t)$  is:

$$G(t) \propto 1/(1 + 4 R_{SD}t)^{1/2} \quad (6)$$

Assuming illumination by a one-dimensional Gaussian beam the above function describes fluorescence recovery due to surface diffusion.<sup>53</sup> In our experiment the focused laser spot bleaches an entire cylindrical cross-section of the tube. Only diffusion



occurring along the length of the nanotube contributes to signal recovery and hence the above equation (6) is valid<sup>31</sup>. The diffusion coefficient  $D$  is included as

$$R_{SD} = D/s^2 \quad (7)$$

where  $s$  is the beam-waist of the focused laser spot  $\propto \exp(-2x^2/s^2)$ .

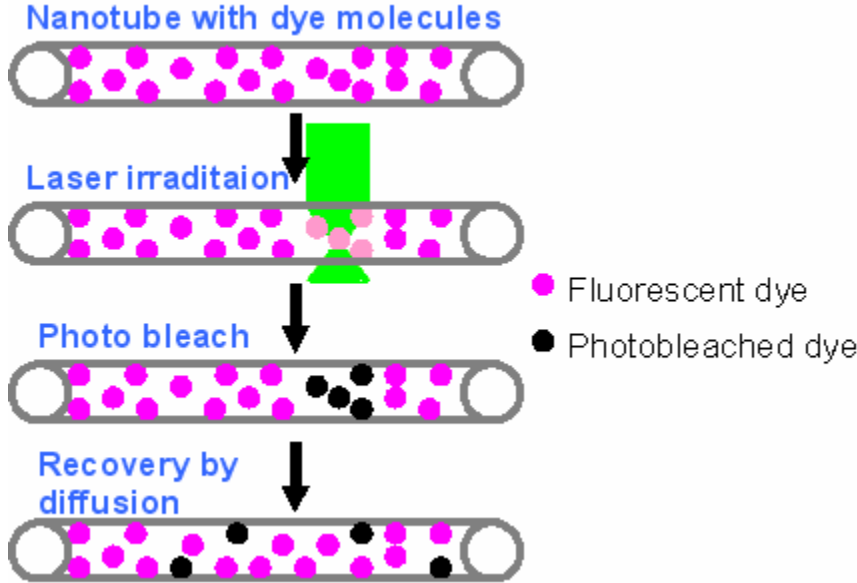


Figure 13. Illustration of FRAP in hydrophobic silica nanotubes.

FRAP measurements were used to measure diffusion coefficients of the entrapped molecules inside nanotubes of inner diameter 170 and 30 nm in a range of water-methanol mixtures. FRAP experiments were conducted over a period of two consecutive days to ensure that equilibrium had been reached for each sample.

### 3.2.3.1 Fast recovery FRAP measurements

Under strongly wetting conditions ( $X_{MeOH} > 0.5$  in the case of both nanotube diameters) rapid modulation of the laser beam was necessary for accurate observation of recovery. In

these experiments an acousto-optic modulator (model C8217A, NEC USA, New York) driven by a Model DE, VCO deflector driver (Intraaction, Bellwood, IL) was used to rapidly adjust the beam intensity. The detector, an avalanche photodiode (APD), was gated to avoid overexposure during photobleaching (high laser intensity). LabView (National Instruments, Austin, TX) was used to synchronize the APD gating and laser intensity.

Acousto-Optic devices are equipments for electronic control of the intensity and position of the laser beam. An Acousto-Optic Modulator (AOM) functions by Bragg scattering light from a periodic density modulation (longitudinal acoustic wave) in a crystal, typically  $\text{TeO}_2$ . When a acoustic wave and lase beam interacts, a refractive index wave is generated tha behaves like a sinusoidal grating and an incident laser beam passing through this grating will get diffracted into several orders. When the alighment is appropriate, the first order beam has the highest efficiency.

An angular rotation mount was used to hold the acousto-optic device for the light beam to intersect the acoustic wave fronts at the Bragg angle. Vertical and horizontal position of the rotatable stage supporting AOM was adjusted so that the laser beam passes through the centers of the entrance and exit apertures of AOM. IntraAction deflector driver is connected to AOM to turn on and off the radio frequency acoustic power. Constant radio frequency is maintained, allowing only the deflected beam to emerge from the modulator. Modulator will be in its off state when no acoustic power is applied and will be switched to its transmissive state by turning on acoustic power. In other words when the acoustic

drive is off, the light in the direction of the deflected beam is zero. The diffracted beam can be identified by turning on and off the RF power to AOM and the diffraction spots can be observed on the laboratory wall. Adjust the knobs of the rotatable mounts until the first order diffracted beam is observed to be much more intense than the undeflected beam. Figure 14 shows the schematic for setting up the AOM for FRAP experiments.

The scanning confocal fluorescence microscope unites the power of high performance optical components with computerized control of the instrument and digital image acquisition to achieve a level of sophistication. Figure 15 shows a schematic of the microscope used for the single nanotube measurements. APD is used to count photons as they emerge from the microscope and imaging is done using LabView. A monochromator and Charge-Coupled Device camera is used for spectroscopic imaging in the solvatochromic experiments.

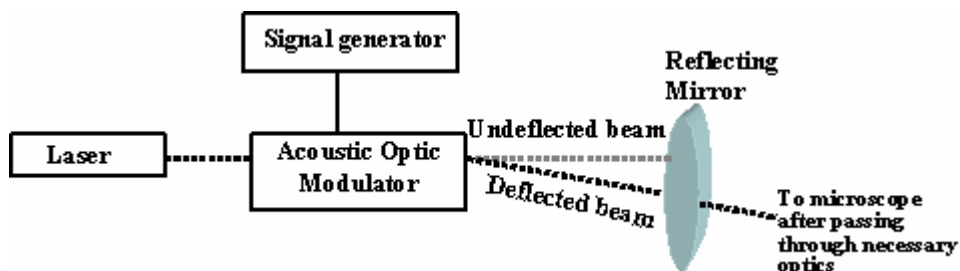


Figure 14. Schematic of modulating the laser beam using Acoustic Optical Modulator.

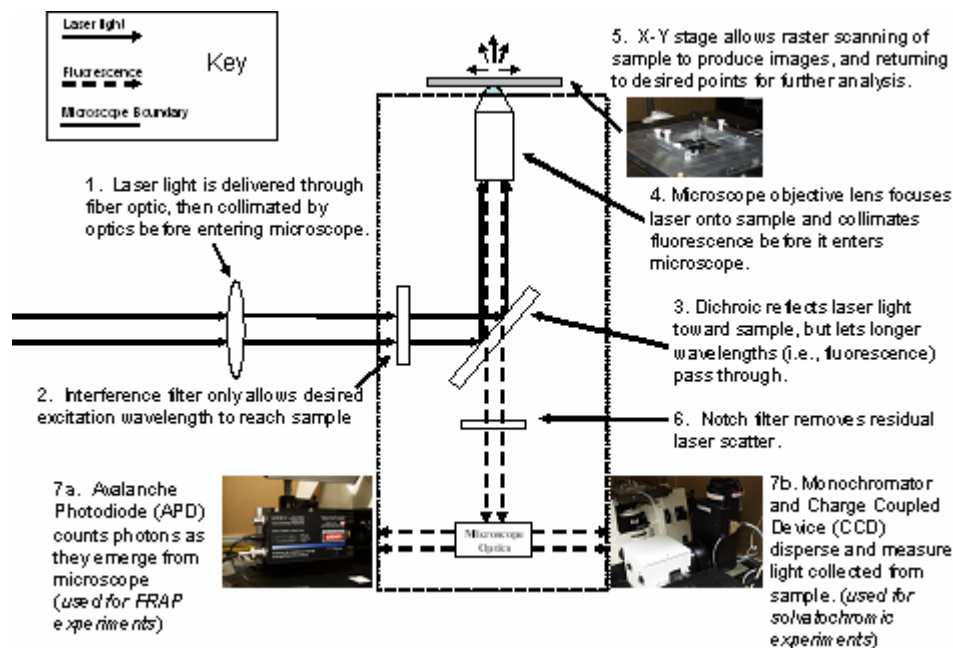


Figure 15. Schematic of scanning confocal fluorescence microscope.

### 3.3 Spectroscopic imaging (Solvatochromic Experiments)

Spectroscopic imaging has been used in which emission spectra are acquired from individual locations on a single nanotube. Spatially resolved fluorescence spectra were collected from individual points in the fluorescence image by positioning the focal point (370 nm FWHM) of the excitation laser at the desired image locations by using a piezo-actuated positioning stage with closed loop feedback (Nanobio II, Mad City Lab, Madison WI). A polychromator (Acton Research Corp., Acton, MA) equipped with a charge-coupled-device (CCD, Roper Scientific, Trenton, NJ) was used to collect and record emission spectra from the microscope image point. Procedure to obtain emission spectra from individual locations on a single nanotube is detailed in Appendix B.

### 3.4 Image analysis

IGOR Pro an extraordinarily powerful and extensible graphing, data analysis is used to obtain all the fluorescence recovery curves and the diffusion coefficient from the series of fluorescence images. Specific FRAP analysis programs were written and incorporated into the IGOR. Appendix C lists the details of IGOR routines.

### 3.5 Transport experiments

Bulk transport experiments with 170 nm hydrophobic nanotube membranes were conducted using a simple U-tube setup described previously.<sup>22,54</sup> Briefly, the nanotube membrane was mounted between the two halves of the U-tube permeation cell. Feed solution was 5 mL of  $4.6 \times 10^{-5}$  M DiIC<sub>18</sub> in the solvent under investigation. Receiver solution was 5 mL of same solvent without DiIC<sub>18</sub>. Both feed and receiver solutions were stirred during permeation experiments and transport occurred across the membrane by diffusion of permeate down the concentration gradient. Transport from feed solution to the permeate solution was monitored by UV-visible absorbance of DiIC<sub>18</sub> using the molar extinction coefficients and wavelengths given in Table 4. Figure 16 (a) shows the schematic for U-tube set up and (B) show the actual setup used for U-tube transport experiments. The extinction coefficients listed in Table 4 for each solvent were obtained by measuring absorbance of each solution (dye in solvent) and constructing calibration curve. Experiments were stopped once 5% of the permeate ion was transported across the membrane from feed to receiver solution. A section of membrane with known surface area ( $0.3165 \text{ cm}^2$  and is equivalent to the area of the circular hole as shown in membrane

assembly) from the actual synthesized membrane and assembled as shown in Figure 16. Transport experiments as briefed above was performed with the same section of membrane for all solvents of interest. After each solvent experiment, the membrane was unmounted from the U-tube halves and washed with the pure solvent to remove all the adsorbed dye molecules and left undisturbed until it is dry and devoid of any permeate ion and used for experiments with next solvent of interest.

Table 4. Molar extinction coefficients and maximum absorption wavelength values ( $\lambda_{\text{max,abs}}$ ) for DiIC<sub>18</sub> at various mole fractions of methanol in water.<sup>52</sup> Reproduced with permission from J. Am. Chem. Soc. 2005, Copyright 2005 Am. Chem. Soc.

$X_{\text{MeOH}}$	$\epsilon$ ( $\text{M}^{-1}\text{cm}^{-1}$ )	$\lambda_{\text{max,abs}}$ (nm)
0.05	45,000	561
0.13	47,000	561
0.31	62,000	549
0.57	98,000	549
1.0	186,000	549

### 3.6 Materials used

Hexanes, concentrated sulfuric acid, and hydrogen peroxide (30%) were purchased from Fisher Scientific. Methanol, glacial acetic acid, and concentrated hydrochloric acid were purchased from J.T. Baker. Silicon(IV) tetrachloride was purchased from ACROS Organics. Octadecyltrimethoxysilane (OTS, 95% purity) was purchased from Gelest Inc. and tetraethoxysilane (TEOS, 99.999% purity) was purchased from Aldrich. For the production of 170 nm inner-diameter nanotubes, commercial alumina membranes

(Anodisc 47, catalogue number 6809-5022) with 0.2  $\mu\text{m}$  pore size were purchased from Whatman. Alumina membranes with 60 nm pores, for the production of 30 nm i.d. nanotubes, were produced in-house. Nile red and 1,1'-dioctadecyl-3,3,3',3'-tetramethylindocarbocyanine perchlorate (DiIC<sub>18</sub>) were purchased from Molecular Probes. Ethanol (95%) was purchased from AAPER Alcohol. All solvents were reagent grade, with the exception of HPLC grade methanol and hexanes, and all were used without further purification.

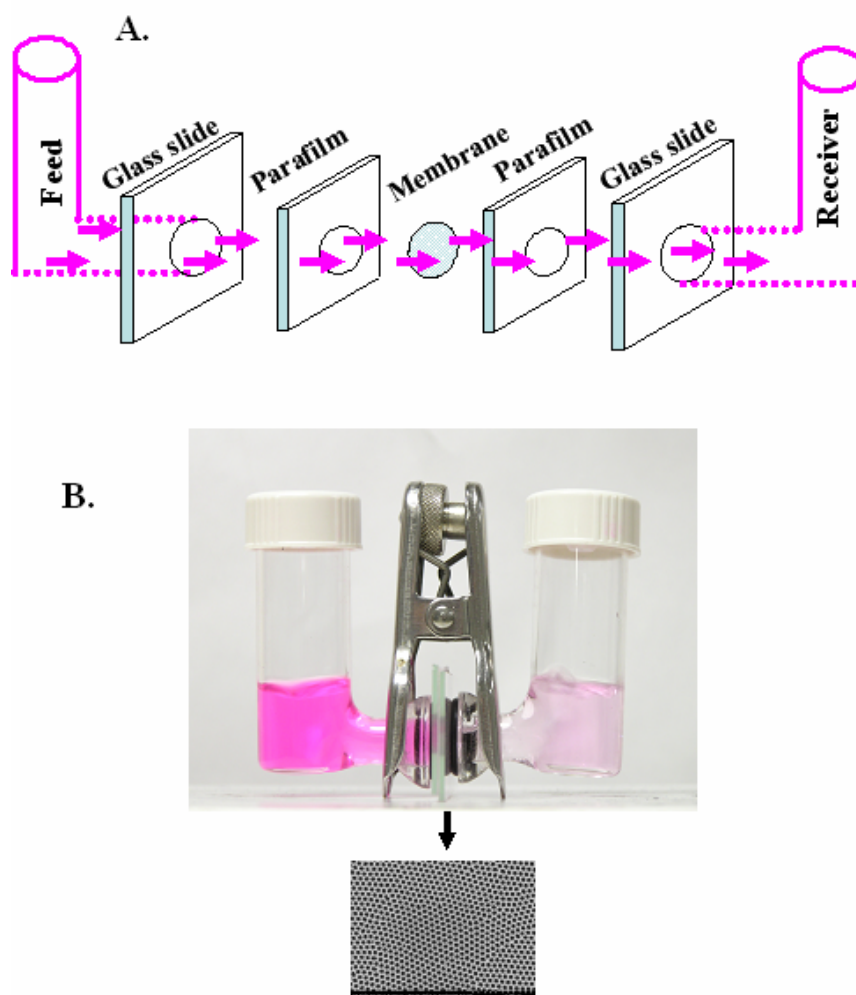


Figure 16. (A) Schematic of membrane assembly and U-tube set up (B) Picture of actual U-tube experiment

## Chapter 4: Results and Discussions

### 4.1 Results

Figure 17A shows the uniform nanotube size distribution (i.d. = 30 nm) obtained using an improved layer-by-layer SSG template synthesis method.<sup>15, 23</sup> These nanotubes were synthesized from a template membrane with a pore diameter of 60 nm and thickness of 12  $\mu\text{m}$ . To achieve a wall thickness of 15 nm, nine layers were sequentially deposited in the SSG process.<sup>15</sup> TEM and confocal fluorescence imaging confirm that the layer-by-layer SSG method provides a higher degree of surface uniformity than our previous method where the wall thickness depended on immersion-time and sol-concentration<sup>31</sup>. The marked improvement in surface homogeneity is seen in the confocal fluorescence image in Figure 17B showing a hydrophobic nanotube containing trace amounts of the fluorophore DiIC<sub>18</sub>. Previously we observed irregularities such as dim or bright regions in fluorescence images of nanotubes which were assigned to inner surface bulges or constrictions.<sup>31, 55</sup> Such irregularities are nearly absent with the new synthesis method. A surprising difference in nanotube lengths was noted when comparing TEM and fluorescence images. In Figure 17A long nanotubes are visible in the TEM image, but such long tubes are never observed in our fluorescence images suggesting that breakage occurs during the sample preparation processes. These processes include introduction of dye to the nanotube interior (Figure 14B) and immobilization of nanotubes on a glass coverslip. During these steps nanotubes are apparently fragmented into shorter pieces. The average length of the nanotubes included in this study was 7  $\mu\text{m}$ .



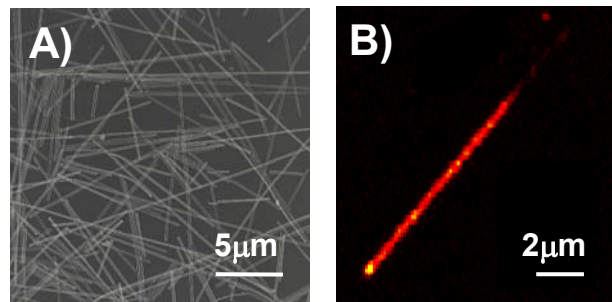


Figure 17. Microscope images of differentially-modified silica nanotubes. (A) A TEM image of nanotubes with 30 nm i.d. and internally modified with OTS (B) Laser scanning confocal fluorescence image of a single 30 nm i.d. nanotube. The interior surface contains a trace amount of the fluorescent dye, DiIC18. Prior to imaging, the nanotube was immobilized on a glass coverslip under water<sup>52</sup>. Reproduced with permission from J. Am. Chem. Soc. 2005, Copyright 2005 Am. Chem. Soc.

#### 4.1.1 FRAP Studies

FRAP experiments were used to monitor the diffusion of adsorbed probe molecules inside an immersed nanotube. A FRAP experiment is conducted by imaging a nanotube in the confocal microscope and then positioning the focused laser beam on a region of the nanotube for 10-20 seconds. The laser intensity is adjusted so that dye molecules in the illuminated spot will undergo rapid and irreversible photochemistry leaving them non emissive, i.e. photobleached. The recovery of the fluorescence signal occurs when unbleached fluorophores diffuse into the bleached region and is a convenient way to measure diffusion of the fluorophore. Figure 18 illustrates the two limiting cases that were observed in FRAP experiments with dye bearing nanotubes. Panels 18A and 18B

are images of a hydrophobic nanotube in *pure water* before and after photobleaching. The four green arrows denote locations where an intense bleaching beam was focused to induce irreversible photobleaching of the local dye molecules. Panel 18A shows the nanotube prior to bleaching. Panel 18B shows the same nanotube imaged 26 minutes after bleaching was completed. In pure water the bleached regions persist indefinitely, indicating that there is *no measurable diffusion of the dye molecules*. Panels 18C and 18D reveal a starkly different behavior when the nanotubes are immersed in *pure methanol*. Here, the *entire nanotube* shows a greatly diminished intensity caused by photobleaching of dye at a single well-defined spot. This effect is due to the *rapid diffusion of the dye molecules* during and subsequent to photobleaching. The rapid exchange of dyes within the laser spot during the bleaching period and diffusion of bleached dye throughout the nanotube results in decreased emission intensity over the entire nanotube. The very different observations from the two solvents are due to their respective wetting strengths at the nanotube interior. In pure water, the absence of diffusion indicates that the nanotube interior is dry. This assignment is supported by observations from single-molecule fluorescence correlation spectroscopy studies which show that DiIC<sub>18</sub> can diffuse freely at the interface between water and a dimethyloctadecylsiloxane surface.<sup>56</sup> Therefore, FRAP should be observed if a water-OTS interface does exist inside of a nanotube. Furthermore, based on predictions and observations of capillarity at the macroscale one should expect that the hydrophobic nanotube interior is dry in water and filled in methanol. For instance, an OTS-coated capillary of 0.5 mm i.d. shows a capillary depression of 0.79 cm in pure water and a rise of 0.88 cm in pure methanol. When the nanotube is filled in methanol it was necessary to

conduct FRAP experiments with a higher temporal resolution than is achievable by acquiring sequential confocal images. Accordingly, experiments were conducted using an acousto-optic modulator to switch the laser intensity, as described in the experimental section. This method provides enough time resolution to achieve an accurate measurement of the fluorescence recovery as shown in Figure 18E. The fluorescence intensity,  $I(t)$ , in Figure 18E was fit to equation 5.<sup>53</sup>  $G(t)$  is given as eq 8 by combining eq 6 and 7.

$$G(t) = \frac{B}{\left(1 + 4 \frac{Dt}{s^2}\right)^{1/2}} \quad (8)$$

where  $B$  is the bleach depth,  $s^2$  is the beam spot variance and  $D$  is the diffusion coefficient of the fluorophore. The diffusion coefficient calculated for the data in Figure 18E is about one third of the value obtained for DiIC<sub>18</sub> on planar C<sub>18</sub>/water interfaces obtained by single-molecule fluorescence correlation spectroscopy.<sup>57, 58</sup> It is interesting that the dye remains within the nanotube even in pure methanol, a good solvent for this dye. The lower diffusion coefficient may reflect stronger adsorption at the curved interface relative to the planar C<sub>18</sub>/water interface and this could explain why the dye remains in the nanotube.

#### *4.1.2 Spectroscopic Imaging*

We used the solvatochromism of Nile red to gauge the local dielectric properties of the OTS-modified nanotube interior surface. Figure 19A contains spectra acquired from Nile red in four different solvents ranging from heptane to a mixture of 2% v/v methanol in

water. As the polarity of the solvent increases, the wavelength of maximum emission ( $\lambda_{\text{max}}$ ) increases. This solvatochromic property is used to provide further confirmation that our nanotube interiors are in fact dry in water and wetted in methanol. Figure 19B shows the emission spectra for Nile red acquired from the same single nanotube immersed first in water and then in methanol. Prior to immersion the emission from this nanotube was collected in air (data not shown) and had a  $\lambda_{\text{max}}$  of 580 nm. The sample cell was then filled with water and the  $\lambda_{\text{max}}$  from the same nanotube was observed to remain unchanged. The values in air and water correspond well to the value measured for Nile red dissolved in the moderately nonpolar solvent ethyl acetate. This similarity suggests that an effective dielectric, determined by the proximities of the OTS alkyl chains, the polar nanotube surface, and the siloxane anchor, is reported by Nile red at the nanotube interior surface. The sample cell was next filled with methanol and the Nile red  $\lambda_{\text{max}}$  value changed to 605 nm. The observed red shift in  $\lambda_{\text{max}}$  indicates that the polarity of the probe environment increased as the nanotube interior filled with methanol. As seen in Figure 19A, Nile red has a  $\lambda_{\text{max}}$  of 638 nm in pure methanol. The lower value of  $\lambda_{\text{max}}$  measured in the nanotube simply indicates that the probe environment is still impacted by the C<sub>18</sub> interface. It is impossible to determine where the Nile red is located relative to the surface, however it may be possible to selectively excite subpopulations of Nile red to distinguish between emission from molecules at the C<sub>18</sub> layer and from those solvated in methanol, and this will be attempted in future work. Additionally, we are currently developing the use of a covalently linked Nile red analogue<sup>51</sup> to allow more accurate determination of the dielectric properties at the nanotube interior interface as a function of immersing solvent.

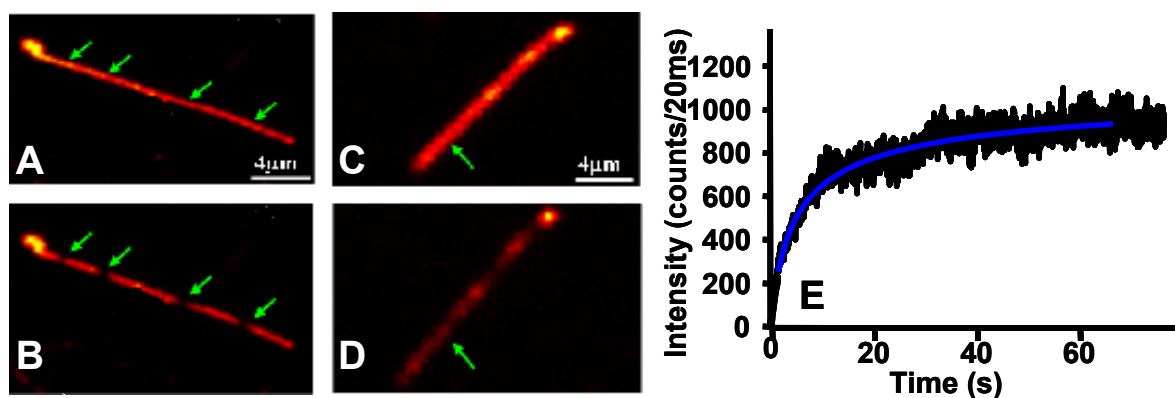


Figure 18. Examples of FRAP experiments conducted with 30 nm i.d. nanotubes under non-wetting conditions in water and strongly-wetting conditions in methanol. (A) Confocal fluorescence image of a DiIC18-bearing hydrophobic nanotube immersed in water just prior to conducting the FRAP experiment. The green arrows indicate four spots which were arbitrarily chosen for photobleaching. (B) A confocal image obtained 26 minutes after photobleaching was conducted showing that under pure water no FRAP is observed. The lack of diffusion-induced recovery suggests that the nanotube interior remains dry when immersed in water as expected for a hydrophobic capillary. (C,D) Confocal images of a hydrophobic nanotube before and after conducting a FRAP experiment in methanol. Here, bleaching was conducted at a single spot shown by the green arrow. In contrast to the experiment conducted in water, a decrease in emission was observed over the entire nanotube interior. The wide-spread bleaching occurs because of rapid diffusion by DiIC18 in the nanotube interior. As molecules are bleached, they rapidly diffuse away diluting the concentration of fluorophores over the entire nanotube. Facile diffusion in the nanotube indicates that hydrophobic nanotube interior has been filled by methanol. (E) Fluorescence recovery curve demonstrating the rapid recovery observed in pure methanol. This data was used to calculate the diffusion coefficient

for DiIC18 in the methanol-filled nanotube by using equations 1,2&4 . The calculated value is  $8.7 \times 10^{-7} \text{ cm}^2/\text{s}$ .<sup>52</sup> Reproduced with permission from J. Am. Chem. Soc. 2005, Copyright 2005 Am. Chem. Soc.

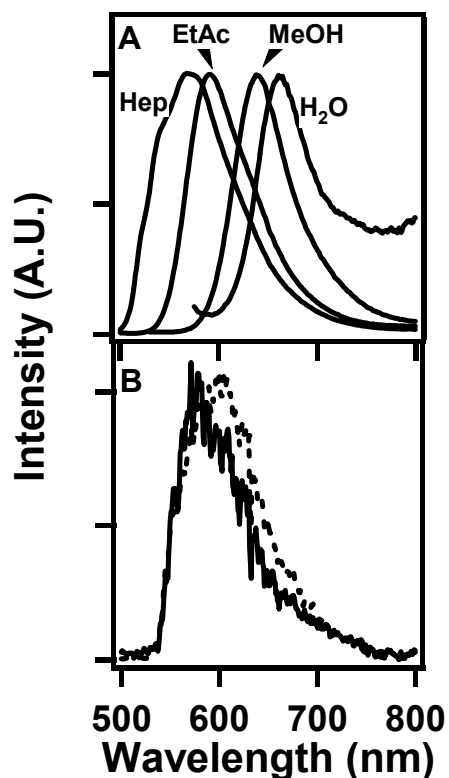


Figure 19. Nile red fluorescence spectra acquired in different solvents and from a single silica nanotube. (A) Nile red emission in heptane, ethyl acetate, methanol and water. In water, a small proportion (2%) of methanol was added to aid dissolution. (B) Emission spectra from Nile red inside an OTS modified nanotube. The nanotube was initially immersed under water (—) and then under methanol (---). The spectrum acquired from the dry nanotube prior to the addition of water (data not shown) overlays well with the spectrum in water.  $\lambda_{\text{max}}$ .<sup>52</sup> Reproduced with permission from J. Am. Chem. Soc. 2005, Copyright 2005 Am. Chem. Soc.

### *4.1.3 Observing Capillary Wetting*

It is apparent from the results thus far that the OTS modified nanotubes remain dry in water and are filled in pure methanol. An important implication of the Young-Laplace theory of capillarity is that sign of the capillary pressure depends only on the contact angle formed between meniscus and the capillary wall. Therefore, in a capillary, one expects to see a discrete transition from non-wetting to wetting when the contact angle drops below  $90^\circ$  and this transition should be independent of capillary size. An important objective of the current work is to determine if these expectations from the Young-Laplace equation hold at the nanoscale. To achieve this end we conducted a systematic study of nanotubes immersed in mixtures over a range of methanol mole fractions. The results of these experiments are shown in Figure 20 where the nanotube wettability is plotted against methanol mole fraction ( $X_{\text{MeOH}}$ ). Note that we have defined wettability as the fraction of experiments in which FRAP was observed. Each point in Figure 18 is calculated from at least 14 FRAP measurements. Wettability values of zero indicate that FRAP was never observed in any of the bleaching experiments. A sharp transition from non-wetting to wetting conditions is observed as predicted by the Young-Laplace equation and there is no significant difference between the two nanotube sizes. During our experiments we made infrequent observations of anomalous wetting observed in the 170 nm i.d. nanotubes at  $0 < X_{\text{MeOH}} < 0.5$  and these observations led to the small, non-zero values of wettability reported at low methanol mole fractions in Figure 20. These anomalous observations result from a few nanotubes with defect and this is discussed in section 4.1.3.1

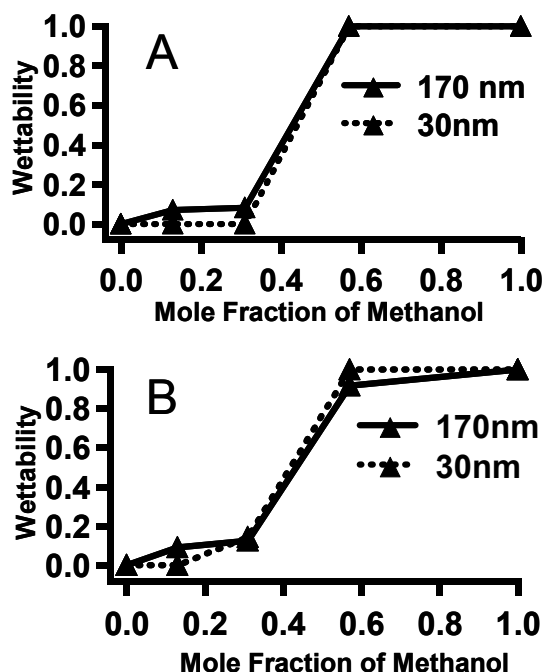


Figure 20. Solvent-dependent wettability of 30 and 170 nm nanotubes. (A) Wettability of the hydrophobic nanotube interior over a range of methanol mole fractions for both 30 and 170 nm nanotube internal diameters. The transition from nonwetting to wetting conditions occurs between 0.31 and 0.57 methanol mole fraction for both nanotube sizes. B) Wettability of both nanotube sizes after equilibration for 24 h.<sup>52</sup> Reproduced with permission from J. Am. Chem. Soc. 2005, Copyright 2005 Am. Chem. Soc.

#### 4.1.3.1 Nanotube Defects and Anomalous Wetting

A small number of nanotubes were wetted at low methanol fractions and these observations led to the unexpected non-zero wetting values observed below  $X_{\text{MeOH}}$  in Figure 20. We have assigned these defects to broken ends which occur during processing of the nanotubes. Defects from breaks should be present exclusively at the nanotube ends. Detailed inspection of our data from individual nanotubes does reveal that FRAP observations responsible for the anomalous wetting at low methanol concentrations came



primarily from data acquired near a nanotube end. If FRAP data collected exclusively from the center of individual nanotubes is analyzed, then calculated wettability is zero for methanol mole fractions below 0.5 in all cases. An example of anomalous FRAP from a nanotube immersed at low methanol concentration ( $X_{\text{MeOH}} = 0.31$ ) is given in Figure 21. In this example, diffusion was recorded near the two nanotube ends. The anomalous wetting of this particular nanotube is likely due to imperfections that are not readily discernible in the fluorescence image and that could have resulted from fragmentation of longer nanotubes. The TEM image of Figure 21B shows an example of a broken nanotube end. The majority of tube ends seen in TEM images do not appear broken. Our current hypothesis is that the jagged ends in a few nanotubes are likely responsible for the anomalous wetting observed below  $X_{\text{MeOH}} = 0.5$ . We previously reported a wettability value of 0.75 for 200 nm i.d. nanotubes immersed for 24 h in solutions with  $X_{\text{MeOH}} = 0.31$ .<sup>31</sup> The previously reported value was an overestimate due to a far greater degree of heterogeneity in nanotube samples prepared with our previous SSG method. As discussed above, layered deposition results in a much more homogeneous sample allowing a better measurement of wetting in nanoscale pores. Figure 20 includes wettability values for 30 nm i.d. nanotubes. These samples show even less anomalous FRAP at low  $X_{\text{MeOH}}$ . This is interpreted as fewer defects, or breaks, for the narrower nanotubes. The cross sectional area of a 30 nm i.d. nanotube consists of 75% silica while that of a 170 nm i.d. nanotube is only 28% silica. The increased wall-to-pore ratio may result in a higher ultimate strength for the narrower tubes.

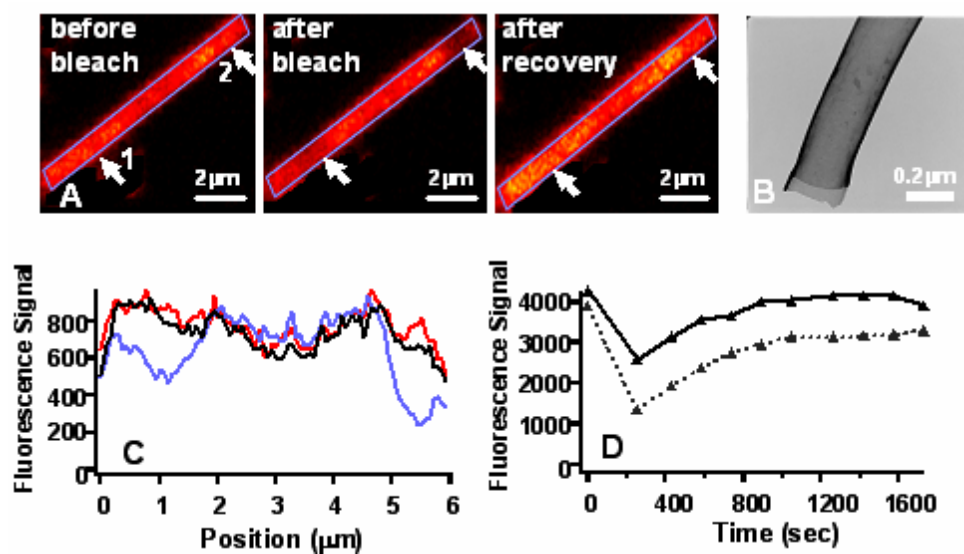


Figure 21. FRAP experiment conducted in a nanotube (i.d. = 170 nm) immersed in a water/methanol mixture, XMeOH = 0.31. (A) A sequence of fluorescent images taken during the FRAP experiment. (B) TEM showing a fragmented nanotube end. (C) Fluorescence intensity profiles taken along the nanotube before bleaching (red), after bleaching (blue) and after recovery (black). (D) FRAP recovery curves constructed from sequential images for point 1 (solid line) and point 2 (dotted line).<sup>52</sup> Reproduced with permission from J. Am. Chem. Soc. 2005, Copyright 2005 Am. Chem. Soc.

#### 4.1.4 Membrane Transport Experiments

Our results from individual nanotube experiments, using FRAP and solvatochromism, provide a detailed view of the wetting behavior in individual nanotubes. These results should be extendable to describe the performance of membranes consisting of arrays of nanotubes. The template synthesis method is readily amenable to testing ensembles of nanotubes; since before final processing, the membrane itself is essentially an array of single nanotubes. Martin and coworkers have tested transport properties of nanotube

membranes<sup>22,50</sup> and we have employed similar techniques to investigate the transport of DiIC<sub>18</sub> across a membrane of 170 nm i.d. pores using the same methanol/water mixtures employed in our single nanotube experiments. DiIC<sub>18</sub> was used in membrane transport experiments so that direct comparison with single nanotube measurements would be valid. The transport experiments are used to measure the rate of DiIC<sub>18</sub> molecules diffusing across a membrane between a stock and receiver solution. Transport is monitored by UV-vis absorption of DiIC<sub>18</sub> in the receiver solution at the absorbance maxima given in Table 4. The molar extinction coefficients in Table 4 were used to calculate the concentrations by Beer's law. Figure 22A shows a comparison between transport measurements made with a nanotube membrane and our single nanotube wettability studies. The transport rate mirrors the wettability. The good correlation between the two sets of experimental data strengthens our conclusion that nanotube wetting does not occur at methanol mole fractions of 0.3 or less.

#### *4.1.5 AC Impedance Measurements*

AC impedance measurements have been widely used to demonstrate ionic conductivity of membranes in aqueous solutions and offer a probe-free method for verifying the wetting behavior of our nanotubes membranes.<sup>54,59,60</sup> Nyquist analysis of impedance data reduces the apparent impedance to an equivalent circuit composed of solution resistance ( $R_S$ ), membrane resistance ( $R_M$ ), and membrane capacitance ( $C_M$ ). From the best fit to the Nyquist plot the  $R_M$  and  $C_M$  values can be obtained. Here, the larger the membrane resistance, the smaller the ionic conductivity of the membrane. Membrane resistance values larger than 1 M $\Omega$ , in aqueous solution imply that the membrane is dry inside since

the ions (e.g.  $K^+$  and  $Cl^-$ ) can not exist inside the nanotubes of the membrane due to their insolubility in the hydrophobic layers. Figure 22B shows a plot of membrane resistance vs. mole fraction of methanol. Over the methanol mole fraction range 0 to 0.31, very large values of  $R_M$ ,  $> 10\text{ M}\Omega$ , were obtained, while the  $R_M$  value transitioned to  $\sim 50\ \Omega$  at 0.57 methanol mole fraction. Interestingly, we found the wetting-dewetting process was reversible, with slight hysteresis. This is consistent with our previous results in which reversible wetting due to spontaneous cavitation was observed.<sup>31</sup>

It may be argued that strong partitioning of the permeant molecule to the hydrophobic nanotube interior could hinder or even facilitate transport. For instance, selective transport of toluene and pyridine through thiol-functionalized gold nanotube membranes has been demonstrated by the Martin group.<sup>19, 61</sup> They proposed a mechanism whereby partitioning of hydrophobic molecules from the aqueous feed solution to the thiol layer facilitates transport across the membrane even though the pores remain unwetted by the water. This mechanism does not apply to our studies since, relative to toluene and pyridine, DiIC<sub>18</sub> has a low vapor pressure, high molecular weight and is a charged molecule. Additionally, the OTS layer on silica is not a well ordered monolayer as is seen for alkyl thiols on gold.

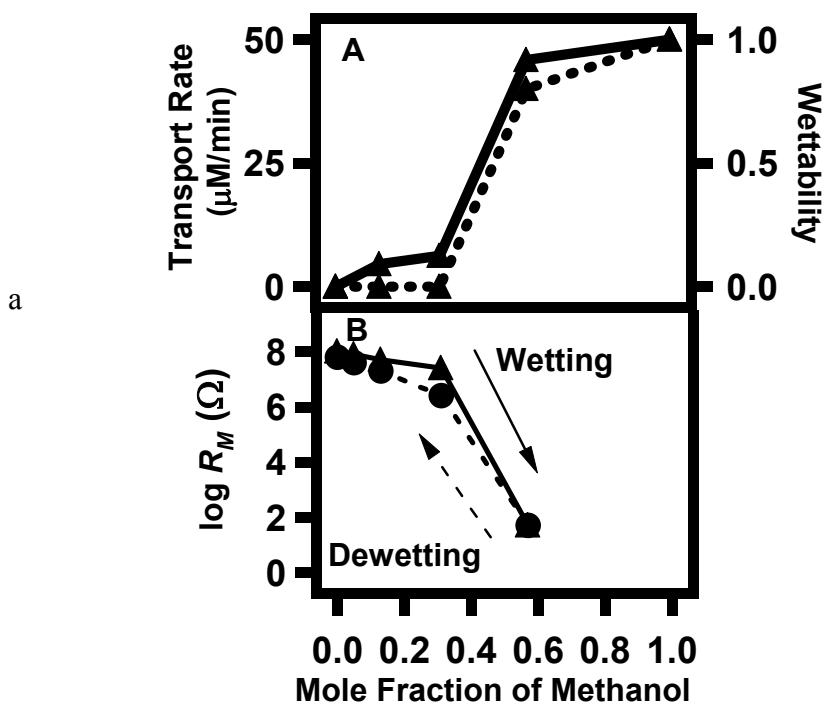


Figure 22. Results from measurements made with an OTS-modified nanotube membrane (i.d. = 170 nm). (A) Comparison of results from solute transport studies (dotted line) with those from wettability studies (solid line) of individual nanotubes. (B) Semilogarithmic plot of the membrane resistance,  $R_M$ , over a range of  $X_{MeOH}$ .  $R_M$  values were determined from AC impedance measurements and were conducted in electrolytic solutions of 0.1 M KCl. The value of  $R_M$  is diminished by ion flow when the membrane pores are wetted and is dramatically increased when the hydrophobic membrane pores are dry. The sharp decrease in the value of  $R_M$  above  $X_{MeOH} = 0.31$  indicates that the membrane channels have filled. During the course of the experiment, methanol concentration was first increased and then decreased. Dewetting was observed as the mole fraction was decreased.<sup>52</sup> Reproduced with permission from J. Am. Chem. Soc. 2005, Copyright 2005 Am. Chem. Soc.

## 4.2 Discussion

Nanotube samples with precise internal pore diameters and known surface chemistries provide a means to examine the behavior of fluids in well-defined nanoscale cylindrical containers, thus allowing us to solve problems relevant to nanofluidics and theoretical aspects of confined liquids. Our previous work focused on evaluating diffusion rates inside 200 nm i.d nanotubes under wetting conditions.<sup>31, 55</sup> Here we examine the wetting process itself, by investigating wettability as a function of both nanotube size and solvent composition and compare our results to prediction from the Young Laplace equation.

In FRAP studies, we use the presence or absence of dye-diffusion in hydrophobic nanotubes as a signature for wetting and non-wetting conditions, respectively. Transport and AC-impedance studies conducted with intact nanotube membranes support our results from studies of individual nanotubes. As expected from conventional capillarity, both 30 and 170 nm i.d. nanotubes show a sharp transition from non-wetting to nonwetting as the mole fraction of methanol increases. The wetting transition, or nanotube filling, occurs near equimolar methanol/water concentrations for both nanotube diameters.

In the following discussion we treat our cylindrical silica nanotubes as capillaries. An approximate treatment of capillarity in macroscopic systems, such as glass capillary tubes, is traditionally made in terms of the Young-Laplace equation. This approach assumes that the contact angle at the liquid/gas/solid interface ( $\theta_c$ ) will determine the concavity of the meniscus at the nanotube opening and that the meniscus is spherical with a radius of curvature equal to the capillary radius,  $r$ . The meniscus formed by a wetting

solution ( $\theta_c < 90^\circ$ ) at the capillary opening will be concave with respect to the nanotube interior and the capillary pressure will be positive. Alternatively the meniscus formed by a non-wetting solution ( $\theta_c > 90^\circ$ ) will be convex with respect to the nanotube interior and the capillary pressure will be negative.

The data in Figure 18 illustrate the limiting behaviors observed in FRAP experiments between nanotubes immersed in pure water vs nanotubes in pure methanol. In pure water, the absence of diffusion indicates that the nanotube interior is dry. This assignment is supported by the Young-Laplace equation and by observations from ordinary capillaries as illustrated in the results section. Therefore, it is not unexpected that the OTS-treated interior of nanotubes would remain dry in pure water regardless of the nanotube diameter. Figure 20 summarizes observations made over a range of methanol mole fraction ( $X_{\text{MeOH}}$ ) and reveals the transition between wet and dry nanotubes.

An obvious question is: does the Young-Laplace equation describe the wettability of our nanotubes? The capillary pressures given in Table 5 were calculated using contact angles measured for water on  $C_{18}$  modified glass coverslip (hydrophobic planar surface). Since a positive capillary pressure promotes filling, nanotube filling should occur at  $X_{\text{MeOH}} > 0.05$ . The results from our wettability studies summarized in Figure 20 show that a clear transition from non-wetting to wetting conditions exists close to  $X_{\text{MeOH}} = 0.5$ , a value approximately ten times greater than that predicted by the Young-Laplace equation. A possible explanation for the observed discrepancy between our experimental results and the theoretical predictions of Table 5 may be that the samples have simply not

equilibrated by the time the measurements are made. To insure that our results reflect equilibrium conditions, we conducted experiments on a single sample over a period of two days. Figure 20B shows the results for samples which were allowed to equilibrate for at least 24 hours. Very little difference is measured between the two days. The entrapment of air inside the nanotubes as they are immersed could provide a possible explanation for the unusual wettability results. However, this argument can be countered since it is unlikely that trapped air would remain in the nanotubes for 24 hours given the gas permeability of the nanotube walls and the immense capillary pressures in Table 5.

Table 5. Contact angles of methanol/water mixtures on an OTS surface and the predicted capillary pressure for 30 and 170 nm nanotubes.<sup>52</sup> Reproduced with permission from J. Am. Chem. Soc. 2005, Copyright 2005 Am. Chem. Soc.

$X_{\text{MeOH}}$	$\theta_c$ (deg) <sup>a</sup>	$\Delta P_{170 \text{ nm}}$ (atm) <sup>b</sup>	$\Delta P_{30 \text{ nm}}$ (atm)
0	102	-3.5	-20
0.05	92	-0.4	-2.4
0.13	76	2.6	15
0.31	65	3.2	18
0.57	34	5.4	31
1	10	5.9	28

*a* Advancing contact angles ( $\theta_c$ ) were measured for each solvent on an OTS-coated glass coverslip. *b* Pressure differences were calculated using eq 3.

The failure of the Young-Laplace equation to predict the wetting behavior of hydrophobic nanotubes is interesting and should be addressed since it obviously impacts a range of potential applications involving nanoscale fluid-based devices. A recent study by Fadeev and coworkers have shown that the Young-Laplace underestimates capillary pressure by as much as a factor of 2 for water in hydrophobic pores of a few



nanometers.<sup>36</sup> Here we have complemented these studies by directly observing the change in capillary pressure that occurs with the addition of a co-solvent.

Theoretical treatments of confined fluids<sup>31, 42, 47</sup> may provide explanations for the failure of conventional capillarity at the nanoscale. These explanations stem from issues of phase stability in confined liquids. Critical diameters for the phase stability of liquid water in slit-like pores has been estimated at  $\sim 100$  nm.<sup>42</sup> In cylindrical pores the critical diameter will be even greater and has been calculated to be as much as several microns.<sup>47</sup> Phase instability occurs when the chemical potentials of the vapor and liquid phase are equal. Spontaneous fluctuations of vapor layers formed near the hydrophobic surface and the surface tension of the solvent can lead to spontaneous cavitation even in a filled volume. In our case, the liquid phase never fills the volume until a much higher methanol mole fraction than predicted by the Young-Laplace equation is reached. Instability of the liquid phase in the hydrophobic pore may be responsible for the discrepancy. It is also possible that the discrepancy could arise from our dependence on macroscopic contact angles acquired from flat surfaces or from changes in the liquids surface tension when the meniscus is highly curved. Sobolev et al. have addressed this issue and shown that surface tension of water in quartz capillaries with radii down to 40 nm is unchanged from that of bulk but find a steep dependence of the observed contact angle on meniscus velocity.<sup>62</sup> Until contact angle and surface tensions at highly curved menisci can be directly measured or accurately calculated, predictions of wettability in nanotubes will rely on parameters gleaned from macroscopic observations or on direct measurements as presented here. We have shown that direct measurement is more reliable.

# Chapter 5: Conclusions and Future Work

## 5.1 Conclusions

We have used an improved SSG template synthesis to prepare silica nanotubes within the pores of alumina template membranes with the means to control the wall thickness. Using this method we produced nanotubes with both 30 and 170 nm i.d. Both sizes were prepared with hydrophobic interior surfaces achieved through covalent attachment of OTS. Wettability of the nanotube interior was investigated using FRAP, solvatochromism, membrane transport and AC-impedance measurements. Results from these experiments provide a quantity of evidence indicating that simple capillarity considerations fail to provide an adequate prediction of the wetting behavior in hydrophobic nanotubes of both 30 and 170 nm internal diameters. A sharp transition that is independent of nanotube size is observed between wetting and nonwetting conditions as expected. However, the transition occurs at a much higher methanol mole fraction than predicted by the Young-Laplace equation. The origin of this discrepancy remains unclear but may be due to our reliance on macroscopic values of contact angles or it may be related to liquid phase instability within the hydrophobic pore. The reversibility of the wetting transition suggests that phase instability may be the primary source of the anomalous wetting behavior.

Our results are critically important for the successful implementation of nanotubes as nanofluidic devices, in separations, and for biomedical applications such as drug delivery, or as miniature reaction vessels. Understanding solvent wetting properties in nanotubes

and how these properties vary from macroscopic models will provide a framework for the design of nanotubes with surface chemistries tailor-made for specific applications. The use of single nanotube measurements provides a detailed view of solvent-nanotube interactions that is unachievable with bulk measurements. Our single-nanotube approach, illustrated here with hydrophobic nanotubes, is a promising new method and is adaptable to investigations using silica nanotubes with a wide range of surface chemistries.

## 5.2 Future work

Covalently linked Nile red analogue will be synthesized and used to accurately determine the dielectric properties at the nanotube interior surface as a function of immersing solvent. Our efforts will be expanded to a wider range of experimental variables to help theoreticians address the question of hydrophobicity in confined environments and wetting at nanoscale. Silica nanotubes with charged interiors will be synthesized to understand the role of electrostatic interactions in solvent transport through single nanotubes and nanotube membranes.

# Appendix

## A. Procedure to conduct FRAP Experiments

1. Switch the microscope to wide field epi-illumination and look for a single nanotube by moving the nano resolution scanning stage. *(Note: To ensure that the nanotube identified on the monitor to appear in the fluorescence imaging, set the laser spot position to the center of the stage (62,62) using the LabView software even before starting to look for nanotubes.)*
2. Take a fluorescence image of the selected nanotube with a weak ( $\sim 0.4$  nW) laser power. *(Note: To make sure that same laser power is used for imaging before and after bleaching, it is a good practice to fix one rotating mirror and just change the other mirror; Alternatively connect the power meter each time and check)*
3. Close the shutter and using the fluorescence image of nanotube on the computer, select a position(x, y) on the nanotube for bleaching and press SIT on the LabView screen.
4. Turn OFF the Avalanche Photo Diode (APD) detector. Rotate the mirrors to set high laser power. Open the shutter. Irradiate the chosen point with high ( $\sim 4$   $\mu$ W) laser power for  $\sim 20$  sec. Close the shutter.
5. Switch back to the same power (approximately) used for taking the image before bleach. Turn ON the APD. Sequentially take fluorescence images (minimum 12 images are recommended if the recovery appears reasonable) *(Note : If the nanotube is at least  $7\mu\text{m}$  and if considerable dyes are present all through the tube , at least three*

*positions(both ends and middle) can be chosen to conduct FRAP. Step 3, 4 & 5 has to be repeated separately for each position. Each position will be considered as individual FRAP experiment, when performing the statistical summary and calculating wettability)*

## **B. Procedure to perform spectroscopic imaging.**

1. Prepare the nanotube sample as detailed in sample preparation on a TEOS coated coverslip and fix a o-ring around the sample to create a sample cell and load it on to the microscope. The sample cell will not have any solvent at this time.
2. Switch the microscope to wide field epi-illumination and look for a single nanotube by moving the nano resolution scanning stage. *(Note: To ensure that the nanotube identified on the monitor to appear in the fluorescence imaging, set the laser spot position to the center of the stage (62,62) using the LabView software even before starting to look for nanotubes.)*
3. Take a fluorescence image of the identified nanotube with a required laser power. Laser with both excitation wavelength 488 nm and 543 nm were tried for solvatochromic experiments.
4. Close the shutter and using the obtained fluorescence image of nanotube on the computer, select a position(x,y) on the nanotube for obtaining emission spectra and press SIT on the LabView screen.

5. Switch the microscope to the polychromator and CCD camera mode . Open the shutter and irradiate the spot for 10 sec and obtain the emission spectra using Spectra Pro software. The emission spectra obtained now is for dry nanotube- air interface. Repeat steps 4&5 again to obtain emission spectra form different positions on the same nanotube.

6. Now carefully fill the sample cell with particular solvent of interest . Ensure that the system is not disturbed to facilitate to image the same nanotube without losing focus. Repeat steps 2 – 5 .

7. Repeat step 6 until all solvents of interest is covered. It is better to seal the top of the ring with another coverslip while using pure methanol as solvent because of it high volatility.

### **C . IGOR routines for loading and manipulating microscope images.**

Following are the IGOR routine names and its use:

1. Image-Tools.ipf for loading and manipulating microscope images. For details see Appendix C1.

2.Spectra-Tools.ipf for loading and manipulating spectra obtained from CCD camera for solvatochromic experiments. For details see Appendix C2.

3. NT-FRAP.ipf for obtaining FRAP recovery curve and diffusion coefficients. For details see appendix C3. Following are the details to be recorded and REQUIRED before using the NT-FRAP.ipf to analyze data for each tube:

1. Range of image numbers (in the LABVIEW) including the image number of before bleach image.

2. The time each image was acquired. This is obtained by right clicking on file properties.
3. Thickness of rectangle to extract cross-section (the thickness of the line drawn to define the nanotube boundary), and bleached area on cross section.
4. x and y position of round and square cursors when the plot line is drawn.
5. Number of bleached points in each tube

### **C1.IGOR routine for loading and manipulating microscope images.**

```
#pragma rtGlobals=1          // Use modern global access method.

//Doug 5-10-02 tools for loading and manipulating microscope images from joes labview
confocal imagingsoftware
//Kenji modified in March, 2003

Menu "SM-Tools" // make menu items
    "&Load_Image", loadmicimage()
    "&Load_Sequential_Images", SeqLoadImages()
    "&Calc_Bead_Width", calc_beadwidth()
    "&Load_Double_Image", loadWimage()
    "&Display_Image", DisplayImage()
    "&Plot_Line", PlotLine()
    "&Bold_Plot_Line", BoldPlotLine()
    "&Clear_Plot_Line", ClearPlotLines()
    "&Make_Movie", Play_Movie()
End

// *****macro for loading an image file saved with joes software //
macro loadmicimage()
    // compatible with Doug's macro
    silent 1
    String File_Name
    variable refnum
    Open /R/T="???" refnum
        FStatus refnum
        File_Name = S_filename
        LoadImage_Core(refnum, File_Name)
    close refnum
    DisplayImage_func(File_Name)
end macro
```

```

function SeqLoadImages()
    string filename
    variable Nfrom, Nto, refNum
    string /G filePrefixI
    string fPrefix = filePrefixI

    Prompt fPrefix, "Prefix of Filename? (for example, \"2004-03-02-I\")"
    Prompt Nfrom, "The Number of Image to Load FROM?"
    Prompt Nto, "The Number of Image to Load TO?"
    DoPrompt "Specify Range of Numbers of Images.", fPrefix, Nfrom, Nto
    if (V_Flag)
        print " loadin file was canceled."
        return -1 // User canceled
    endif
    filePrefixI = fPrefix

    Open /Z=2/R/M="Select Any File in Folder Including Target Files" /T="???"
refNum
    if( V_Flag == -1 ) // file dialog was
canceled
        print " loading files was canceled."
        return -1
    endif
    FStatus refNum
    NewPath /O/Q filePath, S_path
    Close refNum

    variable i
    for( i=Nfrom ; i<=Nto ; i+=1 )
        sprintf filename, "%s%03d", fPrefix, i
        Open /R /P=filePath refnum filename
            FStatus refnum // get
S_filename
                LoadImage_Core(refnum, S_filename)
            Close refnum
        endfor
    end function

function LoadImage_Core(refnum, filename) // load data from file
specified by refnum
    variable refnum
    string filename
    variable image_size, scansize

```



```

        FStatus refnum                                     // get
V_logEOF
    make /O /W /N=(V_logEOF/2) temp
    FBinRead /B=1 /F=2 refnum, temp

    image_size=temp[2]
    scansize=temp[0]/100

    Duplicate/O/R=[image_size,*] temp, $filename         // copy data from
temp to new wave with same name as file
    Redimension/N=(image_size,image_size) $filename     //change from 1-d to
2-d array
    SetScale/P x 0,(scansize/image_size),"", $filename
    SetScale/P y 0,(scansize/image_size),"", $filename
    print filename, ", dwell time = ", temp[1], ": image dimension = ", temp[2], ",
scan range = ", temp[0]/100, "(micron)"
    killwaves temp
end function

macro loadWimage()
    // compatible with Doug's macro
//    silent 1
    String File_Name, wvnm
    variable refnum
    Open /R/T="?????" refnum
        FStatus refnum
        File_Name = S_filename
        LoadWImage_Core(refnum, File_Name)
    close refnum
    sprintf wvnm, "%s_1", File_Name
    DisplayImage_func(wvnm)
    sprintf wvnm, "%s_2", File_Name
    DisplayImage_func(wvnm)
end macro

function LoadWImage_Core(refnum, filename)               // load data from file
specified by refnum
    variable refnum
    string filename
    string wvnm
    variable image_size, scansize
    FStatus refnum                                     // get
V_logEOF
    make /O /W /N=(V_logEOF/2) temp
    FBinRead /B=1 /F=2 refnum, temp

```

```

image_size=temp[2]
scansize=temp[0]/100

sprintf wvnm, "%s_1", filename; print wvnm
Duplicate/O/R=[image_size,image_size*(image_size+1)-1] temp, $wvnm
// copy data from temp to new wave with same name as file
Redimension/N=(image_size,image_size) $wvnm //change from 1-d to
2-d array
SetScale/P x 0,(scansize/image_size),"", $wvnm
SetScale/P y 0,(scansize/image_size),"", $wvnm

sprintf wvnm, "%s_2", filename; print wvnm
Duplicate/O/R=[image_size*(image_size+1),*] temp, $wvnm // copy
data from temp to new wave with same name as file
Redimension/N=(image_size,image_size) $wvnm //change from 1-d to
2-d array
SetScale/P x 0,(scansize/image_size),"", $wvnm
SetScale/P y 0,(scansize/image_size),"", $wvnm
killwaves temp
end function

macro calc_beadwidth(WidthOfFittedGaussianFunction)
variable WidthOfFittedGaussianFunction
print 2 * sqrt(ln(2)) * WidthOfFittedGaussianFunction, "micrometer"
end macro

//===== Display Image
function DisplayImage()
string /G filePrefixI
string /G fileSuffixI
string fPrefix = filePrefixI, fSuffix = fileSuffixI
string wvnm
variable imgNo

Prompt imgNo, "The Number of Image to Display?"
Prompt fPrefix, "Prefix of Filename? (for example, \"2004-03-02-I\")"
Prompt fSuffix, "Suffix of Filename? (for example, \"_A\" or \"_B\")"
DoPrompt "Specify Range of Numbers of Images.", imgNo, fPrefix, fSuffix
if (V_Flag)
print " displaying image was canceled."
return -1 // User canceled
endif
filePrefixI = fPrefix

```

```

fileSuffixI = fSuffix

sprintf wvnm, "%s%03d%s", fPrefix, imgNo, fSuffix
DisplayImage_func(wvnm)
end function

function DisplayImage_func(wvnm)
    string wvnm
    Display/K=1/M/W=(4,4,21,18); AppendImage $wvnm //display, with
location and size specified
    Label left "Microns";DelayUpdate
    Label bottom "Microns"
    ModifyImage $wvnm ctab= {*,*,YellowHot,0} // change color
scheme
    Modifygraph width=250, height=250
    showinfo
    //add cursors
end function

//*****8
function Play_Movie(frames, root, startno,repeat)
    variable frames
    string root
    variable startno, repeat
    Play_Movie_func(frames, root, startno,repeat)
end macro

function Play_Movie_func(frames, root, startno,repeat)
    variable frames
    string root
    variable startno, repeat
    silent 1
    variable i, j, b
    for( j=0 ; j<repeat ; j+=1 )
        for( i=0 ; i<frames ; i+=1 )
            // print i
            AppendImage $root + num2str(startno + i)
            if (i>0)
                RemoveImage $root + num2str(startno+i-1)
            endif
            for( b=datetime+.5 ; datetime<b ; )
                endfor
            endfor
        endfor
    endfor
end function

```

```

// *****Use the cursors to select a line on the image that you wish to plot
DSE 05/24/02
// ===== modified by Kenji
03/25/2003
Macro PlotLine()
    variable x1, x2, y1, y2
    string TopPlot, image
    x1=pcsr(A) ; y1=qcsr(A) ; x2=pcsr(B) ; y2=qcsr(B)
    TopPlot=WinName (0,1)
    image=CsrWave(A, TopPlot)
    BoldPlotLine_Core(image, x1, y1, x2, y2, 0, 3)
end macro

Macro BoldPlotLine(thickness)
    variable thickness
    variable x1, x2, y1, y2
    string TopPlot, image
    x1=pcsr(A) ; y1=qcsr(A) ; x2=pcsr(B) ; y2=qcsr(B)
    TopPlot=WinName (0,1)
    image=CsrWave(A, TopPlot)
    BoldPlotLine_Core(image, x1, y1, x2, y2, thickness, 3)
end macro

Function BoldPlotLine_Core(image, x1, y1, x2, y2, thickness, graph_switch)
    string image
    variable x1, x2, y1, y2
    variable thickness // thickness of additional line on both
side (pixel) // =0 : single line
    variable graph_switch // switch to cross section (=0 : off, =1 : on)
// bit of 1 : draw rectangle in
graph // bit of 2 : display new graph
of cross section
    variable plen, thck
    variable tmpx, tmpy, ttx, tty, dx, dy
    variable i, j
    wave imgwv
    String plotnm, TopPlot
    silent 1
    thck = trunc(thickness)
    plen = max ( abs(y2-y1), abs(x2-x1) ) + 1

```

```

dx = (x2-x1)/(plen-1)
dy = (y2-y1)/(plen-1)
//make /O/N=(125,125) checkwv
//checkwv *= 0
duplicate /O $image, imgwv
make /O/D/N=(plen) plotwv
SetScale /P x 0,(DimDelta(imgwv, 0)*sqrt(dx^2+dy^2)), "", plotwv

for(i=0 ; i<plen ; i+=1)
    tmpx = trunc( x1+i*dx +0.5)
    tmpy = trunc( y1+i*dy +0.5)
    plotwv[i] = imgwv[tmpx][tmpy]
//    checkwv[tmpx][tmpy] += 1
    for(j=1 ; j<=thck ; j+=1)
        ttx = trunc( (tmpx + j*dy) + 0.5)
        tty = trunc( (tmpy - j*dx) + 0.5)
        plotwv[i] += imgwv[ttx][tty]
//        checkwv[ttx][tty] +=1
        ttx = trunc( (tmpx - j*dy) + 0.5)
        tty = trunc( (tmpy + j*dx) + 0.5)
        plotwv[i] += imgwv[ttx][tty]
//        checkwv[ttx][tty] +=1
    endfor
endfor

if( (graph_switch & 1) > 0 )
    TopPlot=WinName (0,1)
    SetDrawLayer /W=$TopPlot ProgAxes
    if(thck == 0)
        // Draw Line of Cross Section
        SetDrawEnv /W=$TopPlot linethick=1.5, linefgc=(30000, 30000,
65000), xcoord=prel, ycoord=prel
        conv_drawline( TopPlot, x1, y1, x2, y2 )
    else
        // Draw Rectangle of ROI
        SetDrawEnv /W=$TopPlot linethick=1.5, linefgc=(30000, 30000,
65000), xcoord=prel, ycoord=prel
        conv_drawline( TopPlot, (x1 + thck*dy), (y1 - thck*dx), (x1 -
thck*dy), (y1 + thck*dx) )
        SetDrawEnv /W=$TopPlot linethick=1.5, linefgc=(30000, 30000,
65000), xcoord=prel, ycoord=prel
        conv_drawline( TopPlot, (x1 + thck*dy), (y1 - thck*dx), (x2 +
thck*dy), (y2 - thck*dx) )
        SetDrawEnv /W=$TopPlot linethick=1.5, linefgc=(30000, 30000,
65000), xcoord=prel, ycoord=prel

```

```

        conv_drawline( TopPlot, (x1 - thck*dy), (y1 + thck*dx), (x2 -
thck*dy), (y2 + thck*dx) )
        SetDrawEnv /W=$TopPlot linethick=1.5, linefgc=(30000, 30000,
65000), xcoord=prel, ycoord=prel
        conv_drawline( TopPlot, (x2 + thck*dy), (y2 - thck*dx), (x2 -
thck*dy), (y2 + thck*dx) )
    endif
endif
plotnm = image + "line"
duplicate /O plotwv, $plotnm
redimension /N=(i*1) $plotnm
if( (graph_switch & 2) > 0 )
    display /K=1 $plotnm
    Label bottom "position (micrometer)"
    showinfo
endif
killwaves plotwv,imgwv
end function

function conv_drawline(TopPlot, x1, y1, x2, y2)
    variable x1,y1,x2,y2
    String TopPlot
    DrawLine /W=$TopPlot (x1+0.5)/125 , 1 - (y1+0.5)/125 , (x2+0.5)/125 , 1 -
(y2+0.5)/125
end function

macro ClearPlotLines()
    String TopPlot
    TopPlot=WinName (0,1)
    SetDrawLayer /K/W=$TopPlot ProgAxes
end macro

//

```

## **C2. IGOR routine for loading and manipulating spectrums obtained from CCD camera for solvatochromic experiments.**

```

#pragma rtGlobals=1          // Use modern global access method.

//Doug 4-3-00 this macro loads princeton instruments spectra files taken from the 1340
pixel ICCD
// as it loads each frame it creates an average wave called avespec, and also an integral
and spectral mean wave

```

```

// called specint and specmean. These waves have a point for each frame. This ipf also
contains a routine for
// autocorrelating spectral mean trajectories in wavenumbers, choose the desired area
with cursors and make sure the
//spectral mean is the target window
//Doug 5-3-00 added filename denotaion to specint, specmean and avespec
//Doug 5-4-00 added ability to do background subtraction of each frame as the mean, and
intensity are calculated.
//checking the background subtraction box means each frame will have the wave bkgnd
subtracted. to use this feature
// I average the frames after bleaching and call this averaged spectrum bkgnd.
//Doug 5-15-00 added standard deviation calculation to the "firstmoment" procedure,
values are stored in stddev wave and can be displayed
//on the specmean wave as error bar
//Kenji 6-29-04 modified to be compatible with higher order of polynomial fitting for
wagelength

```

```

Menu "&CCD-Tools"
    "&Load_Frames" , loadICCDspectra()
    "&Autocorrelate",correlatespectra()
    "&Filter", DiffHist()
End

```

```

Macro loadICCDspectra()
    variable/G StartFrame=0
    variable/G EndFrame
    variable/G FileNumber
    string/G FileName
    variable/G xstart
    variable/G xfactor, xfactor2, xfactor3, xfactor4, xfactor5
    variable/G ROI_Left
    variable/G ROI_Right
    variable/G exposure
    string /G NameExt
    variable/G StartSave=0
    variable/G EndSave

    silent 1;
    Make /O /N=(1340) /D avespec
    avespec=0
    open /D /R /T=".spe" FileNumber
    FileName=s_filename

```

```

//open/R/T=".spe"FileNumber // dialogue to
choose file and set filename reference
open /R FileNumber Filename // open file to
read experiment parameters
Fstatus FileNumber
NameExt=s_filename
FSetPos FileNumber, 1446
FbinRead /F=2 FileNumber, EndFrame //get number of frames in the
file
EndSave=EndFrame
print "scans=" + num2str(EndFrame)

FSetPos FileNumber,10
FbinRead /F=4 FileNumber, exposure //get exposure time in
milliseconds
print "exposure time=" + num2str(exposure) + "seconds"

FSetPos FileNumber, 3263
FbinRead /F=5 FileNumber, xstart //get starting wavelength and
nanometers per pixel
FbinRead /F=5 FileNumber, xfactor
FbinRead /F=5 FileNumber, xfactor2
FbinRead /F=5 FileNumber, xfactor3
FbinRead /F=5 FileNumber, xfactor4
FbinRead /F=5 FileNumber, xfactor5
print "x-start=" + num2str(xstart)
printf "x-factor= (%f, %f, %f, %f, %f)r", xfactor, xfactor2, xfactor3, xfactor4,
xfactor5
close FileNumber //close file
after reading parameters

Make /O /N=1340 /D xaxis
xaxis = xstart + xfactor*(x+1) + xfactor2*(x+1)^2 + xfactor3*(x+1)^3 +
xfactor4*(x+1)^4 + xfactor5*(x+1)^5
display /K=1 /W=(100,100,600,400) avspec vs xaxis
ControlBar 80
showinfo

//top row
SetVariable SetvarStart pos={0,0},size={120,20}, frame=1, font="times",
value=StartFrame //these lines
SetVariable SetvarFrames pos= {125,0},size={120,20}, frame=1, font="times",
value=EndFrame //put menu items on
SetVariable Setvar0 pos= {250,0},size={120,20}, frame=1, font="times",
value=ROI_Left //display window

```



```

        SetVariable Setvar1 pos= {380,0},size={120,20}, frame=1, font="times",
value=ROI_Right
        //second row
        SetVariable SetvarStartSave pos={0,30},size={120,20}, frame=1, font="times",
value=StartSave
        SetVariable SetvarEndSave pos= {125,30},size={120,20}, frame=1,
font="times", value=EndSave
        CheckBox CheckUpdate, noproc, pos={300,30}, size={80,15},title="Update?",
value=0
        CheckBox CheckSaveWaves, noproc, pos={390,30},
size={80,15},title="SaveTrajectories?", value=1
        //Third Row
        Button GetSpec, pos={0,55} ,size={100,20}, proc=getSpectra, title="Get
Spectra"
        CheckBox CheckSave, noproc, pos={120,55}, size={80,15},title="saveframes?",
value=0
        CheckBox CheckBkgnd, noproc, pos={210,55},
size={80,15},title="subtractbackground?", value=0
        CheckBox CheckMakeBkgnd, noproc, pos={350,55},
size={80,15},title="MakeBkgndFile?", value=0

        SetVariable SetvarExt pos= {480,55},size={200,20}, frame=1, font="times",
value=NameExt
end macro

```

```

//*****

```

```

Macro getSpectra(ctrlName)
    string ctrlName

    variable i=StartFrame
    variable j=0
    variable NormAve
    Make /O /N=(EndFrame)/D specmean
    Make /O /N=(EndFrame)/D specint
    Make /O /N=(EndFrame)/D specmax
    Make /O /N=(140)/I MeanHist
    Make /O /N=(EndFrame)/D stddev
    stddev=0
    specint=0
    specmean=0
    specmax=0
    NormAve=0
    avespec=0

    string TextBoxString

```

```

        sprintf TextBoxString, "%s\raverage of %d Frames\r exposure time=%d",
NameExt, EndSave-StartSave, exposure
        Textbox /C /N=text0 /F=0 /S=3 /A=LT TextBoxString
        Textbox /C /N=text1 /F=0 /S=3 /A=RT "max=\rmean="
        controlinfo CheckUpdate // check to see
if update? is checked or not
        if(V_Value==1)
                PauseUpdate
        endif
        do
                GBLoadWave/Q/B/T={80,80}/S=(4100+i*1340*2)/W=1/U=1340
FileName // load a frame from spe file
                Make /O /N=(1340) /U/I $(S_fileName+num2str(i))

                //$(S_fileName+num2str(i))=$( "wave"+ num2str(j))
                $(S_fileName+num2str(i))=$( "wave"+ num2str(0))
                killwaves wave0
//                SetScale/P x xstart,xfactor,"", $(S_fileName+num2str(i))

                controlinfo CheckBkgnd
                if(V_Value==1)
                        // check to see if bkgnd should be
subtracted
                        $(S_fileName+num2str(i))=$(S_fileName+num2str(i))-bkgnd
                        // subtract the wave called bkgnd from the current frame
                endif

                if ( (i>StartSave-1)%& (i<EndSave+1))
                        // average only frames from StartSave to
EndSave
                avespec+=$(S_fileName+num2str(i))
                NormAve+=1
                endif

                //wavestats/Q $(S_fileName+num2str(i))
                //specmax[i]=V_maxloc

                //firstmoment($(S_fileName+num2str(i)),xstart,(xstart+(383*xfactor)),i,'specmean',
'n','specint') //
                firstmoment( $(S_fileName+num2str(i)), stddev, ROI_Left, ROI_Right, i,
'specmean', 'specint' )

                controlinfo CheckSave //
check to see if checksave is checked or not

```

```

        if(V_Value==0)
            killwaves $(S_fileName+num2str(i)) //delete individual frames if
checksave is not checked
        endif
        i+=1
        j+=1
    while ( i<EndFrame )

//kill_waves(0,j)

avespec=avespec/NormAve

Histogram/B={560,1,140}/R=[StartSave,Endsave] specmean,MeanHist

SetScale/P x xstart,xfactor,"", avespec
SetScale/P x 0,exposure,"", specmean
SetScale/P x 0,exposure,"", specint
SetScale/P x 0,exposure,"", specmax

    controlinfo CheckMakeBkgnd //
check to see if MakeBkgnd is checked or not
    if(V_Value==1)
        Duplicate/O avespec,bkgnd //copy avespec into bkgnd
    endif
    controlinfo CheckSaveWaves // check to see
if MakeBkgnd is checked or not
    if(V_Value==1)
        Duplicate/O specmean, $("specmean"+NameExt)
        Duplicate/O specint, $("specint"+NameExt)
        Duplicate/O avespec, $("avespec"+NameExt)
        Duplicate/O specmax, $("specmax"+NameExt)
        Duplicate/O MeanHist, $("MeanHist"+NameExt)
    endif

end macro

//This macro kills waves that are named wave* where *=some integer, it will ask for start
and stop integers
//that correspond to wave(start)and wave(stop)

Macro kill_waves(start,stop)
    variable start
    variable stop

```

```

string temp
silent 1
do
    temp="wave"+num2str(start)
    killwaves $temp
    start+=1
while (start<stop)
end maco

```

//This function calculates the total number of points under a wave, the integral of the wave  
//and the position of the firstmoment (i.e. centroid) of the wave

```

function firstmoment(wavename,deviation,xbegin, xend,iii,outw,outw2)
    wave wavename, deviation
    variable xbegin, xend, iii
    wave outw, outw2

    variable totalpoints, integral, i, startpt, endpt, weightedsum, mean

    totalpoints=0
    startpt = x2pnt( 'wavename', xbegin )
    endpt = x2pnt( 'wavename', xend )
    i = startpt

    integral = area( 'wavename', xbegin, xend )
    do
        totalpoints += abs( 'wavename'[i] )
        weightedsum += abs( 'wavename'[i] * pnt2x( 'wavename', i ) )
        i += 1
    //    print num2str('wavename'[i])
    while ( i < endpt )
    //    print "totalpoints="+ num2str(totalpoints)
    //    print "integral="+num2str(integral)
    //    print "firstmoment="+num2str(weightedsum/totalpoints)
    outw[iii] = weightedsum / totalpoints
    outw2[iii] = integral
    mean = weightedsum / totalpoints
    i = startpt
    do
        deviation[iii] += ( (pnt2x('wavename', i) - mean) ) * 'wavename'[i]
        i += 1
    while ( i < endpt )

```

```

        deviation[iii] = sqrt( abs(deviation / totalpoints) )

end

//*****
//converts a spectral mean trajectory in nanometers to an autocorrelation function in
//wavenumbers of the form
// <nu(o)nu(t)-<nu>^2

function correlatespectra()
variable Apos
variable Bpos

variable i
i=0
killwaves/z correlation // deletes correlation if it
exists // read postion of cursors to
Apos=xcsr(A) // read postion of cursors to
determine data to copy
Bpos=xcsr(B)

duplicate /O/R=(Apos,Bpos) CsrWaveRef(A), correlation //put selected data in
correlation

'correlation'=1/('correlation'*1e-7) //convert to wavenumbers
wavestats 'correlation' // get average and number or points,
in V_avg and V_npnts
correlate/C 'correlation', 'correlation' // does circular autocorrelation
//correlate 'correlation', 'correlation' // does circular autocorrelation
'correlation'='correlation'/V_npnts-V_avg^2
duplicate/O correlation, tmpwave
do
    tmpwave[V_npnts-i-1]=correlation[i]
    i+=1
while(i<V_npnts)
duplicate/O tmpwave,correlation
SetScale/P x,-.2 ,.2,"", correlation
end

```

### C3. IGOR routine for obtaining FRAP recovery curve and diffusion coefficients.

```
#pragma rtGlobals=1          // Use modern global access method.

Menu "NT-FRAP-Analysis" // make menu items
    "&Nanotube FRAP Analysis", doAnalyze()
    "&Plot Cross Section", plotCrossSection()
    "&Plot Recovery Curves", plotRecoveryCurves()
    "&Convert from 'tm' to 'sc'", tm2sc()
//    "&Set File Prefix", NT_SetFilePrefix()
End

function NT_SetFilePrefix()
//    set file prefix, for example "2004-02-02-I"
    string str
    Prompt str, "File Prefix? (for example \"2004-02-02-I\")"
    DoPrompt "Input file prefix", str
    if (V_Flag)
        return -1 // User canceled
    endif
    string /G filePrefixI = str
end function

////////// Main Function //////////
function doAnalyze()
    string /G filePrefixI
    string fPrefix = filePrefixI
    variable i, s, t, iFrom, iTo, csx1, csy1, csx2, csy2, sitNo, Thck, Width
    string twvnm, osxwvnm, osywvnm, wvnm

    Prompt fPrefix, "Prefix of Image Files (for example, \"2001-02-03-I\")?"
    Prompt t, "The Number of Tube?"
    Prompt iFrom, "The Number of Image before Bleach?"
    Prompt iTo, "The Number of Last Image?"
    DoPrompt "Input Experimental Information", fPrefix, t, iFrom, iTo
    if (V_Flag)
        print " Analys is canceled."
        return -1 // User canceled
    endif
    filePrefixI = fPrefix
    printf " Tube %d: from image %d to %d\r", t, iFrom, iTo

    sprintf twvnm, "t%d_nm", t
```

```

sprintf osxwvnm, "t%d_osX", t
sprintf osywvnm, "t%d_osY", t
make /O /N=(iTo-iFrom+1) $twvnm, $osxwvnm, $osywvnm
wave twv = $twvnm, osxwv = $osxwvnm, osywv = $osywvnm
for( i = 0 ; i <= (iTo-iFrom) ; i+=1 )
    twv[i] = iFrom + i
endfor
osxwv = 0 ;          osywv = 0

Prompt csx1, "x-Position of Round Cursor?"
Prompt csy1, "y-Position of Round Cursor?"
Prompt csx2, "x-Position of Square Cursor?"
Prompt csy2, "y-Position of Square Cursor?"
Prompt sitNo, "How many Bleached Points on This Tube?"
Prompt Thck, "Thickness of Rectanble to Extract Cross Section?"
Prompt Width, "Wdith of Bleached Area on Cross Section?"
DoPrompt "Input Information", csx1, csy1, csx2, csy2, sitNo, Thck, Width
if (V_Flag)
    print " Analys is canceled."
    return -1 // User canceled
endif
printf "  cursor position: (%d, %d)-(%d, %d) thickness: %d\r", csx1, csy1, csx2,
csy2, Thck
printf "  No. of bleaching points: %d  width of bleached area: %d\r", sitNo,
Width

make /O /N=(sitNo) sX, sY

variable bx, by
string diaStr
for( s = 0 ; s < sitNo ; s += 1 )
    bx = 0 ;          by = 0
    sprintf diaStr, "x-Position of %s Bleached Point?", noStr(s+1)
    Prompt bx, diaStr
    sprintf diaStr, "y-Position of %s Bleached Point?", noStr(s+1)
    Prompt by, diaStr
    sprintf diaStr, "Input Information of %s Bleached Ppoints.", noStr(s+1)
    DoPrompt diaStr, bx, by
    if (V_Flag)
        print " Analys is canceled."
        return -1 // User canceled
    endif
    sX[s] = bx
    sY[s] = by
    printf "  position of %s bleached point: (%d, %d)\r", noStr(s+1), bx, by
endfor

```

```

variable DC=2, cRange=10 // range to take correlation
Prompt DC, "Do You Want to Compensate Lateral Drift of Smaple?" popup,
"Yes; No"
Prompt cRange, "If YES, specify the range"
DoPrompt "Specify Drift Compensation.", DC, cRange
if (V_Flag)
    print " Analys is canceled."
    return -1 // User canceled
endif
if( DC == 2 )
    cRange=0
endif
printf " drift shift sompensation is "
if( cRange == 0 )
    printf "off\r"
else
    printf "on - range is %d\r", cRange
endif

sprintf wvnm, "%s%03d", fPrefix, twv[0]
BoldPlotLine_Core( wvnm, csx1, csy1, csx2, csy2, Thck, 0 )
doSection( t, csx1, csy1, csx2, csy2, Thck, cRange, fPrefix, "" )
SectionGraph( t, fPrefix, "" )
for( s=0 ; s<sitNo ; s+=1 )
    doPlot( t, s, csx1, csy1, csx2, csy2, sX[s], sY[s], Width, fPrefix, "" )
endfor
RecoveryGraph( t )
sprintf wvnm, "t%d_nm", t
edit /K=1 $wvnm
sprintf wvnm, "t%d_tm", t
AppendToTable $wvnm
sprintf wvnm, "t%d_sc", t
AppendToTable $wvnm
killwaves sX, sY
end function

function /S noStr(no)
variable no
string str
if( no==1 )
    str = "1st"
elseif( no==2 )
    str = "2nd"
elseif( no==3 )

```



```

        str = "3rd"
    else
        sprintf str, "%dth", no
    endif
    return str
end function

function doSection(tubeNo, X1, Y1, X2, Y2, thck, cRange, prefix, suffix)
    variable tubeNo, x1, y1, x2, y2, thck, cRange
    string prefix, suffix
    variable n, nTo
    string bsnm, wvnm

    make /O /N=2 pos

    sprintf wvnm, "t%d_nm", tubeNo
    wave wv_no = $wvnm
    sprintf wvnm, "t%d_osX", tubeNo
    wave wvosx = $wvnm
    sprintf wvnm, "t%d_osY", tubeNo
    wave wvosy = $wvnm

    sprintf bsnm, "%s%03d%s", prefix, wv_no[1], suffix // set Base
    wave name0
    wavestats /Q wv_no
    nTo = V_npnts
    BoldPlotLine_Core(bsnm, x1+wvosx[1], y1+wvosy[1], x2+wvosx[1],
y2+wvosy[1], thck, 0)
    for( n=2 ; n<nTo ; n+=1 )
        sprintf wvnm, "%s%03d%s", prefix, wv_no[n], suffix
        if( WaveExists($wvnm) == 0 )
            printf " error: wave '%s' does not exist.\r", wvnm
            continue
        endif
        correlate_image(bsnm, wvnm, cRange, pos) // take
    Correlation
        pos[0] += wvosx[1];        pos[1] += wvosy[1]
        wvosx[n] = pos[0];        wvosy[n]=pos[1]
        BoldPlotLine_Core(wvnm, x1+pos[0], y1+pos[1], x2+pos[0], y2+pos[1],
thck, 0)
    endfor
    killwaves pos
end function

function doPlot(tubeNo, sitNo, X1, Y1, X2, Y2, sitX, sitY, thck, filePrefix, fileSuffix)

```

```

variable tubeNo, sitNo, X1, Y1, X2, Y2, sitX, sitY, thck
string filePrefix, fileSuffix
variable n, Nto
string wvnm
variable q1, q2, len, x0, x

sprintf wvnm, "t%d_nm", tubeNo
wave wv_no = $wvnm

// Get Position
//      print X1, Y1, X2, Y2, sitX, sitY
      q1 = atan2(Y2-Y1, X2-X1)
      q2 = atan2(sitY-Y1, sitX-X1)
      len = sqrt( (sitX-X1)^2 + (sitY-Y1)^2 ) * cos(q1-q2) / sqrt( (X2-X1)^2 +
(Y2-Y1)^2 )
      printf " tube:%d sit:%d pos:%f\r", tubeNo, sitNo+1, max( abs(X2-X1),
abs(Y2-Y1) ) * len
      x0 = floor( max( abs(X2-X1), abs(Y2-Y1) ) * len + 0.5 )
// end Get Position
wavestats /Q wv_no
Nto = V_npnts
sprintf wvnm, "t%d_rc%d", tubeNo, sitNo+1
make /O /N=(V_npnts) $wvnm
wave temp = $wvnm
for( n=0 ; n<Nto ; n+=1 )
    sprintf wvnm, "%s%03d%sline", filePrefix, wv_no[n], fileSuffix
    if( WaveExists($wvnm) == 0 )
        printf " error: wave '%s' does not exist.\r", wvnm
        continue
    endif
    wave cs = $wvnm
    temp[n] = 0
    for( x=x0-thck ; x<=x0+thck ; x+=1 )
        temp[n] += cs[x]
    endfor
endfor
end function

```

```

function correlate_image(wvnm1, wvnm2, range, resWave)
string wvnm1, wvnm2
variable range
wave resWave
variable isize=125
variable xc, yc, xo, yo, val=0, count=0, res=0, xr, yr

```

```

wave wv1 = $wvnm1
wave wv2 = $wvnm2

if( range == 0 )
    return 0
endif

// make /O/N=2 'pnt'
// make /O/N=(range*2+1,range*2+1) checkwv
// checkwv *= 0

for( yc=-range ; yc<=range ; yc+=1 )
for( xc=-range ; xc<=range ; xc+=1 )
    for( yo=range ; yo<(isize-range) ; yo+=1 )
    for( xo=range ; xo<(isize-range) ; xo+=1 )
        val += wv1[xo][yo] * wv2[xo+xc][yo+yc]
        count += 1
    endfor
endfor
val /= count
if( val > res )
//         res = val ;    pnt[0] = xc;           pnt[1] = yc
//         res = val ;    resWave[0] = xc;       resWave[1] = yc
endif
//         checkwv[xc+range][yc+range] = val
//         val = 0;           count = 0;
endfor
endfor
// print xr, yr, res
end function

```

```

function SectionGraph(tNo, filePrefix, fileSuffix)
    variable tNo
    string filePrefix, fileSuffix
    string wvnm, leg, secnm

    sprintf wvnm, "t%d_nm", tNo
    wave temp = $wvnm
    sprintf wvnm, "%s%03d%sline", filePrefix, temp[0], fileSuffix
    sprintf secnm, "t%d_section0", tNo
    duplicate /O $wvnm, $secnm

    sprintf wvnm, "%s%03d%sline", filePrefix, temp[1], fileSuffix
    sprintf secnm, "t%d_section1", tNo
    duplicate /O $wvnm, $secnm

```

```

    wavestats /Q temp
    sprintf wvnm, "%s%03d%sline", filePrefix, temp[V_npnts-1], fileSuffix
    sprintf secnm, "t%d_section2", tNo
    duplicate /O $wvnm, $secnm

    PlotCrossSection_func( tNo )
end function

macro PlotCrossSection( NumberOfTube )
    variable NumberOfTube
    PlotCrossSection_func( NumberOfTube )
end macro

function PlotCrossSection_func( tNo )
    variable tNo
    string secnm, leg

    sprintf secnm, "t%d_section0", tNo
    display /K=1 $secnm
    SetAxis/A/E=1 left
    ModifyGraph lsize($secnm)=1.5, rgb($secnm)=(0,0,65280)
    sprintf leg, "\\s('%s') before bleach", secnm
    TextBox /N=text0/J/A=MC leg

    sprintf secnm, "t%d_section1", tNo
    AppendToGraph $secnm
    ModifyGraph lsize($secnm)=1.0, rgb($secnm)=(0,0,0)
    sprintf leg, "\\s('%s') after bleach", secnm
    AppendText leg

    sprintf secnm, "t%d_section2", tNo
    AppendToGraph $secnm
    ModifyGraph lsize($secnm)=1.5, rgb($secnm)=(65280,0,0)
    sprintf leg, "\\s('%s') after recovery", secnm
    AppendText leg

    Label left "fluorescence signal (photon counts)"
    Label bottom "position (micrometer)"
end function

function RecoveryGraph( tNo )
    variable tNo
    string xwv, wvnm

```

```

variable s, c

sprintf xwv, "t%d_sc", tNo
if( WaveExists($xwv) == 0 )
    sprintf wvnm, "t%d_nm", tNo
    duplicate $wvnm, $xwv
endif
sprintf wvnm, "t%d_tm", tNo
if( WaveExists($wvnm) == 0 )
    duplicate $xwv, $wvnm
endif
plotRecoveryCurves_func( tNo )
end function

macro plotRecoveryCurves( NumberOfTube )
    variable NumberOfTube
    plotRecoveryCurves_func( NumberOfTube )
end macro

function plotRecoveryCurves_func( tNo )
    variable tNo
    string xwv, wvnm, leg
    variable s, c

    make /O/N=5, rcl, gcl, bcl
    rcl = { 65280, 0, 0, 0, 65280 }
    gcl = { 0, 0, 39168, 0, 0 }
    bcl = { 0, 65280, 0, 0, 52224 }

    sprintf xwv, "t%d_sc", tNo
    if( WaveExists($xwv) == 0 )
        print " error: wave does not exist."
        return -1
    endif
    sprintf wvnm, "t%d_rc1", tNo
    c=0
    s=1
    do
        if( s == 1 )
            Display /K=1 $wvnm vs $xwv
            SetAxis/A/E=1 left
            sprintf leg, "\\s('%s') %d", wvnm, 1
            TextBox /N=text0/J/A=MC leg
        else
            AppendToGraph $wvnm vs $xwv
            sprintf leg, "\\s('%s') %d", wvnm, s

```

```

                AppendText leg
            endif
            ModifyGraph mode($wvnm)=4, lsize($wvnm)=1.5, rgb($wvnm)=( rcl[c],
gcl[c], bcl[c] )
            c+=1
            if(c>4)
                c=0
            endif
            s += 1
            sprintf wvnm, "t%d_rc%d", tNo, s
            while( waveexists($wvnm) == 1 )
                Label left "fluorescence signal (photon counts)"
                Label bottom "time (sec.)"
                killwaves rcl, gcl, bcl
            end function

```

```

macro tm2sc( TheNumberOfTube )
    variable TheNumberOfTube
    tm2sc_func( TheNumberOfTube )
end macro

```

```

function tm2sc_func(bn)
    variable bn
    string file_Prefix="t"
    string wvnm
    variable Nto, n

    sprintf wvnm, "%s%d_tm", file_Prefix, bn
    duplicate /O $wvnm, wv
    duplicate /O $wvnm, wvsc
    wavestats /Q wv
    Nto = V_npnts
    make /O /N=(Nto) hour, minu, sec
    hour[0] = floor(wv[0] / 10000)
    minu[0] = floor( (wv[0]-hour[0]*10000) / 100)
    sec[0] = wv[0] - hour[0]*10000 - minu[0]*100
    wvsc[0] = 0
    for( n=0 ; n<Nto ; n+=1 )
        hour[n] = floor(wv[n] / 10000)
        minu[n] = floor( (wv[n]-hour[n]*10000) / 100)
        sec[n] = wv[n] - hour[n]*10000 - minu[n]*100
        wvsc[n] = 3600*(hour[n]-hour[0]) + 60*(minu[n]-minu[0]) + (sec[n]-
sec[0])
    endfor
    sprintf wvnm, "%s%d_sc", file_Prefix, bn

```

```

duplicate /O wvsc, $wvnm
killwaves wv, wvsc, hour, minu, sec
end function

```

```

Function NT_FRAP(w,t) : FitFunc

```

```

    Wave w

```

```

    Variable t

```

```

    //CurveFitDialog/ These comments were created by the Curve Fitting dialog.

```

```

    Altering them will

```

```

    //CurveFitDialog/ make the function less convenient to work with in the Curve
    Fitting dialog.

```

```

    //CurveFitDialog/ Equation:

```

```

    //CurveFitDialog/ f(t) = B - A / ( 1 + 4 * D * (t-t0) / s^2 )^0.5

```

```

    //CurveFitDialog/ End of Equation

```

```

    //CurveFitDialog/ Independent Variables 1

```

```

    //CurveFitDialog/ t

```

```

    //CurveFitDialog/ Coefficients 5

```

```

    //CurveFitDialog/ w[0] = B

```

```

    //CurveFitDialog/ w[1] = A

```

```

    //CurveFitDialog/ w[2] = D

```

```

    //CurveFitDialog/ w[3] = t0

```

```

    //CurveFitDialog/ w[4] = s

```

```

    return w[0] - w[1] / ( 1 + 4 * w[2] * (t-w[3]) / w[4]^2 )^0.5

```

```

End

```

```

//

```

## References

1. Park, O. U. B. S. The Basics of Nanotechnology <http://www.begbroke.ox.ac.uk/nano/accessWeb/index.html>
2. Silbergliitt, R., Nanomaterials: New Trends. In *In Dekker encyclopedia of Nanoscience and Nanotechnology*, schawarz, J. A., Conmtescu,C.I. , Putyera,K., eds., Ed. Taylor and Francis Group: New York, 2004.
3. Martin, C. R., Nanomaterials - a Membrane-Based Synthetic Approach. *Science* **1994**, 266, (5193), 1961-1966.
4. Martin, C. R.; Kohli, P., The emerging field of nanotube biotechnology. *Nature Reviews Drug Discovery* **2003**, 2, (1), 29-37.
5. Gasparac, R.; Kohli, P.; Mota, M. O.; Trofin, L.; Martin, C. R., Template synthesis of nano test tubes. *Nano Letters* **2004**, 4, (3), 513-516.
6. Cho, S. I.; Kwon, W. J.; Choi, S. J.; Kim, P.; Park, S. A.; Kim, J.; Son, S. J.; Xiao, R.; Kim, S. H.; Lee, S. B., Nanotube-based ultrafast electrochromic display. *Advanced Materials* **2005**, 17, (2), 171-+.
7. Rao, C. N. R.; Nath, M., Inorganic nanotubes. *Dalton Transactions* **2003**, (1), 1-24.
8. Che, G.; Lakshmi, B. B.; Martin, C. R.; Fisher, E. R.; Ruoff, R. S., Chemical vapor deposition based synthesis of carbon nanotubes and nanofibers using a template method. *Chemistry of Materials* **1998**, 10, (1), 260-267.
9. Kohli, P.; Harrell, C. C.; Cao, Z. H.; Gasparac, R.; Tan, W. H.; Martin, C. R., DNA-functionalized nanotube membranes with single-base mismatch selectivity. *Science* **2004**, 305, (5686), 984-986.
10. Son, S. J.; Reichel, J.; He, B.; Schuchman, M.; Lee, S. B., Magnetic nanotubes for magnetic-field-assisted bioseparation, biointeraction, and drug delivery. *Journal of the American Chemical Society* **2005**, 127, (20), 7316-7317.
11. Menon, L., Nanoarrays Synthesized from Porous Alumina In *In Dekker encyclopedia of Nanoscience and Nanotechnology*, schawarz, J. A., Conmtescu,C.I. , Putyera,K., eds., Ed. Taylor and Francis Group: New York, 2004.
12. Michal Lahav, T. S. A. V. I. R., Nanoparticle Nanotubes. *Angewandte Chemie International Edition* **2003**, 42, (45), 5576-5579.
13. Kohli, P.; Martin, C. R., Smart nanotubes for biotechnology. *Current Pharmaceutical Biotechnology* **2005**, 6, (1), 35-47.
14. Kohli, P.; Wharton, J. E.; Braide, O.; Martin, C. R., Template synthesis of gold nanotubes in an anodic alumina membrane. *Journal of Nanoscience and Nanotechnology* **2004**, 4, (6), 605-610.
15. Kovtyukhova, N. I.; Mallouk, T. E.; Mayer, T. S., Templated surface sol-gel synthesis of SiO<sub>2</sub> nanotubes and SiO<sub>2</sub>-insulated metal nanowires. *Advanced Materials* **2003**, 15, (10), 780-+.
16. Wirtz, M.; Parker, M.; Kobayashi, Y.; Martin, C. R., Template-synthesized nanotubes for chemical separations and analysis. *Chemistry-a European Journal* **2002**, 8, (16), 3573-3578.



17. Li, A. P.; Muller, F.; Birner, A.; Nielsch, K.; Gosele, U., Hexagonal pore arrays with a 50-420 nm interpore distance formed by self-organization in anodic alumina. *Journal of Applied Physics* **1998**, 84, (11), 6023-6026.
18. Lakshmi, B. B.; Patrissi, C. J.; Martin, C. R., Sol-gel template synthesis of semiconductor oxide micro- and nanostructures. *Chemistry of Materials* **1997**, 9, (11), 2544-2550.
19. Cepak, V. M.; Hulteen, J. C.; Che, G. L.; Jirage, K. B.; Lakshmi, B. B.; Fisher, E. R.; Martin, C. R.; Yoneyama, H., Chemical strategies for template syntheses of composite micro- and nanostructures. *Chemistry of Materials* **1997**, 9, (5), 1065-&.
20. Lakshmi, B. B.; Dorhout, P. K.; Martin, C. R., Sol-gel template synthesis of semiconductor nanostructures. *Chemistry of Materials* **1997**, 9, (3), 857-862.
21. Kohli, P.; Martin, C. R., Smart nanotubes for biomedical and biotechnological applications. *Drug News & Perspectives* **2003**, 16, (9), 566-573.
22. Lee, S. B.; Martin, C. R., Electromodulated molecular transport in gold-nanotube membranes. *Journal of the American Chemical Society* **2002**, 124, (40), 11850-11851.
23. Hou, S. F.; Harrell, C. C.; Trofin, L.; Kohli, P.; Martin, C. R., Layer-by-layer nanotube template synthesis. *Journal of the American Chemical Society* **2004**, 126, (18), 5674-5675.
24. Eisenstein, M., An attractive alternative. *Nature Methods* **2005**, 2, (7), 484-484.
25. Hou, S. F.; Wang, J. H.; Martin, C. R., Template-synthesized DNA nanotubes. *Journal of the American Chemical Society* **2005**, 127, (24), 8586-8587.
26. Library, S. P. Special photo techniques. [www.sciencephoto.com](http://www.sciencephoto.com)
27. Martin, C. R. <http://www.chem.ufl.edu/~crmartin/index.html>
28. Olympus Theory of Confocal Microscopy. [www.olympusfluoview.com](http://www.olympusfluoview.com)
29. Sprague, B. L.; Pego, R. L.; Stavreva, D. A.; McNally, J. G., Analysis of Binding Reactions by Fluorescence Recovery after Photobleaching. *Biophys. J.* **2004**, 86, (6), 3473-3495.
30. Lippincott-Schwartz, J.; Altan-Bonnet, N.; Patterson, G. H., Photobleaching and photoactivation: following protein dynamics in living cells. *Nature Cell Biology* **2003**, S7-S14.
31. Okamoto, K.; Shook, C. J.; Bivona, L.; Lee, S. B.; English, D. S., Direct observation of wetting and diffusion in the hydrophobic interior of silica nanotubes. *Nano Letters* **2004**, 4, (2), 233-239.
32. Fletcher, K. A.; Storey, I. A.; Hendricks, A. E.; Pandey, S.; Pandey, S., Behavior of the solvatochromic probes Reichardt's dye, pyrene, dansylamide, Nile Red and 1-pyrenecarbaldehyde within the room-temperature ionic liquid bmimPF(6). *Green Chemistry* **2001**, 3, (5), 210-215.
33. Adamson, A. W., Gast, A. P., *Physical Chemistry of Surfaces*. John Wiley & Sons: New York: 1997.
34. Limited, K. I. Contact Angle: Basic Concepts. <http://www.ksvltd.com/content/index/applicationnotes>
35. Limited, K. I. Surface and Interfacial Tension: Basic Concepts. <http://www.ksvltd.com/content/index/applicationnotes>
36. Helmy, R.; Kazakevich, Y.; Ni, C. Y.; Fadeev, A. Y., Wetting in hydrophobic nanochannels: A challenge of classical capillarity. *Journal of the American Chemical Society* **2005**, 127, (36), 12446-12447.

37. Wood, J.; Sharma, R., Interaction Forces between Hydrophobic Mica Surfaces. *Journal of Adhesion Science and Technology* **1995**, 9, (8), 1075-1085.
38. Ball, P., Chemical physics: How to keep dry in water. *Nature* **2003**, 423, (6935), 25-26.
39. Chandler, D., Hydrophobicity: Two faces of water. *Nature* **2002**, 417, (6888), 491-491.
40. Hummer, G.; Garde, S.; Garcia, A. E.; Paulaitis, M. E.; Pratt, L. R., Hydrophobic effects on a molecular scale. *Journal of Physical Chemistry B* **1998**, 102, (51), 10469-10482.
41. Hummer, G.; Rasaiah, J. C.; Noworyta, J. P., Water conduction through the hydrophobic channel of a carbon nanotube. *Nature* **2001**, 414, (6860), 188-190.
42. Lum, K.; Chandler, D.; Weeks, J. D., Hydrophobicity at small and large length scales. *Journal of Physical Chemistry B* **1999**, 103, (22), 4570-4577.
43. Lum, K.; Luzar, A., Pathway to surface-induced phase transition of a confined fluid. *Physical Review E* **1997**, 56, (6), R6283-R6286.
44. Maibaum, L.; Chandler, D., A coarse-grained model of water confined in a hydrophobic tube. *Journal of Physical Chemistry B* **2003**, 107, (5), 1189-1193.
45. Waghe, A.; Rasaiah, J. C.; Hummer, G., Filling and emptying kinetics of carbon nanotubes in water. *Journal of Chemical Physics* **2002**, 117, (23), 10789-10795.
46. Forsman, J.; Jonsson, B.; Woodward, C. E.; Wennerstrom, H., Attractive surface forces due to liquid density depression. *Journal of Physical Chemistry B* **1997**, 101, (21), 4253-4259.
47. Giaya, A.; Thompson, R. W., Water confined in cylindrical micropores. *Journal of Chemical Physics* **2002**, 117, (7), 3464-3475.
48. Giaya, A.; Thompson, R. W., Observations on an equation of state for water confined in narrow slit-pores. *Journal of Chemical Physics* **2002**, 116, (6), 2565-2571.
49. Masuda, H.; Fukuda, K., Ordered Metal Nanohole Arrays Made by a 2-Step Replication of Honeycomb Structures of Anodic Alumina. *Science* **1995**, 268, (5216), 1466-1468.
50. Lee, S. B.; Mitchell, D. T.; Trofin, L.; Nevanen, T. K.; Soderlund, H.; Martin, C. R., Antibody-based bio-nanotube membranes for enantiomeric drug separations. *Science* **2002**, 296, (5576), 2198-2200.
51. Martin-Brown, S. A.; Fu, Y.; Saroja, G.; Collinson, M. M.; Higgins, D. A., Single-molecule studies of diffusion by oligomer-bound dyes in organically modified sol-gel-derived silicate films. *Analytical Chemistry* **2005**, 77, (2), 486-494.
52. Jayaraman, K.; Okamoto, K.; Son, S. J.; Luckett, C.; Gopalani, A. H.; Lee, S. B.; English, D. S., Observing Capillarity in Hydrophobic Silica Nanotubes. *J. Am. Chem. Soc.* **2005**, 127, (49), 17385-17392.
53. Thompson, N. L.; Burghardt, T. P.; Axelrod, D., Measuring Surface Dynamics of Biomolecules by Total Internal-Reflection Fluorescence with Photobleaching Recovery or Correlation Spectroscopy. *Biophysical Journal* **1981**, 33, (3), 435-454.
54. Steinle, E. D.; Mitchell, D. T.; Wirtz, M.; Lee, S. B.; Young, V. Y.; Martin, C. R., Ion channel mimetic micropore and nanotube membrane sensors. *Analytical Chemistry* **2002**, 74, (10), 2416-2422.

55. Okamoto, K.; Jayaraman, K.; Son, S. J.; Lee, S. B.; English, D. S., In *In Dekker encyclopedia of Nanoscience and Nanotechnology*; Schwarz, J. A.; Contescu, C. I.; Putyera, K., Eds. Taylor and Francis Group: New York: New York, 2004.
56. Wirth, M. J.; Swinton, D. J., *Anal. Chem* **1998**, *70*, 5264.
57. Wirth, M. J.; Swinton, D. J., Single-molecule probing of mixed-mode adsorption at a chromatographic interface. *Analytical Chemistry* **1998**, *70*, (24), 5264-5271.
58. Korlach, J.; Schwille, P.; Webb, W. W.; Feigenson, G. W., Characterization of lipid bilayer phases by confocal microscopy and fluorescence correlation spectroscopy. *Proceedings of the National Academy of Sciences of the United States of America* **1999**, *96*, (15), 8461-8466.
59. Ikematsu, M.; Iseki, M.; Sugiyama, Y.; Mizukami, A., Oscillatory Phenomena in Model Membrane - Electrical Oscillation in Lipid-Impregnated Membrane-Filter Induced by Alamethicin and Controlled by Bacteriorhodopsin. *Biosystems* **1995**, *35*, (2-3), 123-128.
60. Ding, L.; Li, J. H.; Dong, S. J.; Wang, E. K., Supported phospholipid membranes: Comparison among different deposition methods for a phospholipid monolayer. *Journal of Electroanalytical Chemistry* **1996**, *416*, (1-2), 105-112.
61. Hulteen, J. C.; Jirage, K. B.; Martin, C. R., Introducing Chemical Transport Selectivity into Gold Nanotubule Membranes. *Journal of the American Chemical Society* **1998**, *120*, (26), 6603-6604.
62. Sobolev, V. D.; Churaev, N. V.; Velarde, M. G.; Zorin, Z. M., Surface Tension and Dynamic Contact Angle of Water in Thin Quartz Capillaries. *J. Colloid Interface Sci.* **2000**, *222*, 51-54.